HER🌑N

Contents

THE STABILITY OF TIMBER PORTAL FRAMES
AND ARCH FRAMES
An investigation into the twist-bend buckling stability
of structural frames, of constant rectangular
cross-section, resiliently supported by bracings

G. M. van Erp
Eindhoven University of Technology
Department of Structural Engineering

present address:
Witteveen + Bos
Consulting Engineers
P.O. Box 233, 7400 AE Deventer
The Netherlands

Publications in HERON since 1970

Abstract

The stability of timber portal frames and arch frames with respect to twist-bend buck-
ling (lateral torsional buckling) was studied with the aid of a finite element program.
Frames of rectangular cross-section, resiliently supported by bracings elsewhere in the
structure, were investigated.

The stability of timber portal frames and arch frames

An investigation into the twist-bend buckling stability of structural frames, of constant rectangular cross-section, resiliently supported by bracings

1 Introduction

One of the trends in present-day construction practice is towards the increasingly slender and accurate design of loadbearing structures. This trend is apparent in timbre construction practice too. Partly because of modern fabrication and glueing techniques it has become possible, at acceptable cost, to go a long way towards minimizing the material comsumption in timber structures. Laminated portal frames and arch frames are an important example of this. Although these frames are extensively used, there are still may unanswered questions concerning their lateral stability, particularly with regard to twist-bend buckling. This subject will be examined in the present article basing itself on research which formed part of the author's graduation work at the Eindhoven University of Technology.

2 Statement of the problem

Consider an ideally plane portal frame or arch frame whose moment of inertia in the lateral direction is very much smaller than in the plane of bending. If such a frame is loaded in its plane in torsion-free bending combined with shear and/or axial force, a plane state of equilibrium will primarily be established. If the frame is subjected to a small lateral translation U and a small rotation φ about its longitudinal axis, while the load is still small, and if the cause of this imposed translation and rotation is then removed, the frame will return to its original state. Thus, one stable state of equilibrium is associated with this loading. If the load is further increased, however, a laterally deflected and twisted (torsionally distorted) state of equilibrium becomes possible when the load reaches a certain value. If the frame is then subjected to a lateral displacement and a rotation, this new state of equilibrium will remain even after the cause of this deformation of the frame is removed. Therefore, more than one state of equilibrium is possible. The critical load on a structure is defined as the load at which more than one state of equilibrium can exist. With further increase of the lateral displacement U and the angular rotation φ the load P will steadily increase, decrease or remain constant.

The possible relations between P, U and φ for an ideally plane structure are indicated by the dotted lines in Fig. 1. In actual practice, however, a structure will never be ideally plane or have ideally straight members, but will always have a certain initial deformation. Therefore the relation between P, U and φ in reality will be represented by curves such as those drawn as solid lines in Fig. 1.
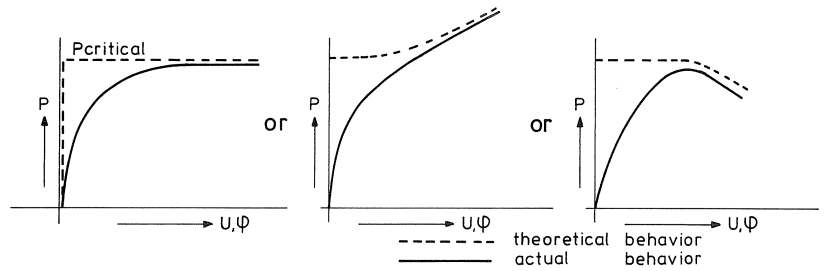
3

Fig. 1.   Possible relation between P, U and φ.

Although the twist-bend buckling (or lateral torsional buckling) of straight and curved beams has been dealt with in numerous publications, the stability of laterally supported portal frames and arch frames with regard to this type of buckling has as yet scarcely been investigated.

As such frames are, with few exceptions, components of a larger structure, laterally unsupported frames seldom occur in practice. In the great majority of cases the lateral displacement of the frames which occurs when overall instability of the structure develops is counteracted by stability-promoting arrangements elsewhere in the structure. These arrangements usually consist of wind bracings (see Fig. 2).

A substantial saving in construction material can be effected by taking the lateral support from the bracings into account, and for this reason the behaviour of laterally supported frames certainly merits investigation.

The research reported here was confined to investigating the "theoretical" twist-bend buckling behaviour of portal frames and arch frames which are laterally supported by bracings or other such stabilizing arrangements. The effect of dimensional deviations, etc. will not be considered in connection with this theoretical behaviour.
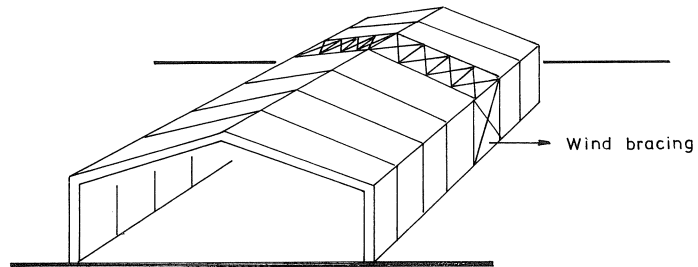

Fig. 2.   Building with three-hinged frames and wind bracing.

3   Portal frames

3.1   *Frames investigated*

The investigation was confined to the component units (halves) of three-hinged portal frames. For practical reasons the number of variables comprised in the investigation has been limited, and in connection with this approach the following assumptions have been made:

4

- The restraining influence that one half frame can exert on the other during twist-bend instability is neglected (in other words, the safe assumption is made that the two half frames will buckle simultaneously in the same direction).
- The displacement of the wind bracing at the knee of the frame is neglected.
- Any torsional restraint exerted by the roof structure on the frame is neglected.
- The frame is of constant rectangular cross-section.
- With regard to the three-hinged portal frame as a whole the effects due to the change in slope of the wind bracing at the top hinge are left out of account.

Since the influence of the one half frame on the other during twist-bend instability (buckling) is neglected, the analysis can be confined to one half.

The gable-type portal frame that was adopted as the starting point for this research is of constant rectangular cross-sectional shape and is supported along the upper edge of the roof beam by a wind bracing attached to it by hinged connections (see Fig. 3). With regard to the forces acting within the plane of the portal frame, the half frame under consideration is provided at A with a hinge and at B with a roller bearing that allows "rolling" movement along the chord A-B. With regard to out-of-plane forces the structure is provided at A with a fork bearing $(U = \varphi = 0)$, while at B the section can rotate freely. Displacement of the roof beam out of the plane of the frame is restrained by the wind bracing. This bracing, which can be regarded as a supporting girder loaded in bending, is provided with a roller bearing at the knee of the frame (point C), so that displacement perpendicular to the plane of the frame is prevented at that point. At D the supporting girder is provided with a bearing which develops flexural restraint but allows displacement perpendicularly to the plane of the frame. The purlins which connect the frame to the bracing are hinged both to the frame and to the bracing. The column of the portal frame is not laterally supported.
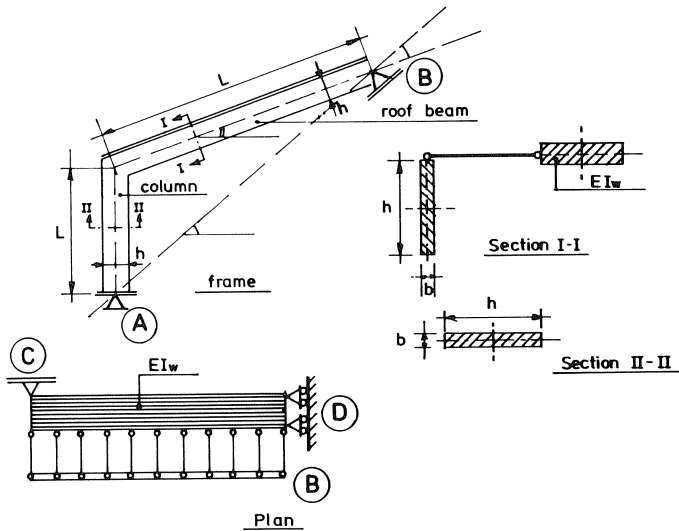

Fig. 3.   Schematic representation of the frame investigated.

3.2 *Loading*

In this investigation it is assumed that the specified loading which causes the largest negative bending moment at the knee of the frame is the most dangerous bending moment with regard to twist-bend instability. In order to find out what load combination causes this largest negative moment, the specified loading of three-hinged portal frames was subjected to a closer analysis. This showed that, depending on the slope and span of the roof, in one case the combinatiom of live load + dead load and in the other case the combination of wind load + dead load is the governing condition.

The bending moment diagram which occurs in the relevant half frame under wind load + dead load remains negative in all parts thereof, whereas with the other load combination there is a positive area in the diagram near the upper end of the roof beam (see Fig. 4). Since a negative moment produces compression at the unsupported edge of the beam, it is more dangerous with regard to twist-bend instability than a positive moment. For this reason the present investigation has been based on the bending moment diagram for the load conbination of wind load + dead load. This condition will, in those cases where the combination with live load causes the largest negative moment at the knee of the frame, constitute a lower bound for the critical loading.

The bending moment diagram due to the combination of wind load + dead load closely resembles the bending moment diagram due to the application of a compressive force acting along the chord A-B of the half frame (see Fig. 4). As this last-mentioned loading case is much simpler to describe, the load adopted as the basis for this twist-bend buckling analysis is a compressive force whose line of action corresponds to the chord.

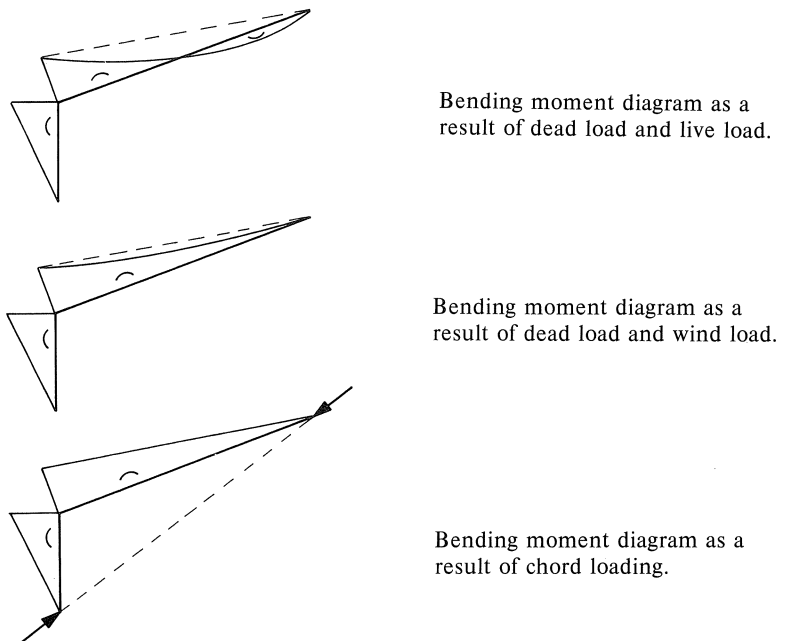Bending moment diagram as a result of dead load and live load.

Bending moment diagram as a result of dead load and wind load.

Bending moment diagram as a result of chord loading.

Fig. 4.   Bending moment diagrams for different types of loading.

6

3.3 Differential equations

For the type of frame under consideration it is possible to derive, both for the roof beam and for the column, the differential equations which describe the twist-bend buckling behaviour. These derivations can be based on equilibrium or on energy considerations. The latter approach was chosen because, with the method which uses the calculus of variations and the principle of minimum potential energy, it is possible in one and the same operation to derive the differential equations and the boundary conditions to be satisfied.

The following assumptions have been made:
- The structure consists of a homogeneous isotropical material, and the laws of Hooke and Bernoulli are valid.
- The deformations within the plane of the structure are negligibly small.
- The cross-sectional shape does not change during twist-bend buckling.
- The loading does not change its direction of action.
- The effect of shear deformation and deformation due to axial force is neglected.

For the roof beam and the column this approach yields the following two sets of coupled differential equations (see Appendix A):
a. roof beam:

$$EI_y u'''' + EI_w \left(u'''' + \tfrac{1}{2} h\varphi'''' \right) + \left(M_x \cdot \varphi \right)'' + P \cos v \cdot u'' = 0 \tag{1}$$

$$EC_w \varphi'''' + EI_w \left(u'''' + \tfrac{1}{2} h\varphi'''' \right)\tfrac{1}{2}h - GI_t \cdot \varphi'' + P \cos v \, \frac{I_p}{A} \, \varphi'' + M_x u'' = 0 \tag{2}$$

b. column:

$$EI_y u'''' + \left(M_x \cdot \varphi \right)'' + P \sin \gamma \cdot u'' = 0 \tag{3}$$

$$EC_w \varphi'''' - GI_t \cdot \varphi'' + P \sin \gamma \, \frac{I_p}{A} \, \varphi'' + M_x \cdot u'' = 0 \tag{4}$$

At the knee of the frame these two sets of differential equations are coupled to each other by means of compatibility and equilibrium conditions.

3.4 Numerical solution

Because it did not prove possible to find analytical solutions that satisfied the boundary conditions it was decided to make use of computer facilities in dealing with the differential equations derived.

With this type of problems the computer can be used in two fundamentally different ways: the differential equations can be solved numerically or, alternatively, a finite element program capable of solving geometrically non-linear problems can be applied.

For the present purpose the latter alternative was chosen, for the following reasons:
- The basis for the former alternative (i.e., numerical solution) is provided by the differential equations in which, for simplification, certain influences have been neglect-

ed which are automatically included in a finite element program, such as deformation due to shear and axial force, stress concentrations at the inner edge of the knee, and possible deformation of the cross-section during twist-bend buckling.
- The availability, at the Eindhoven University of Technology, of a finite element program with which geometrically non-linear problems can be analysed.
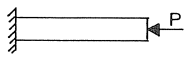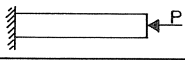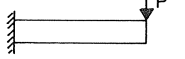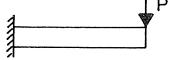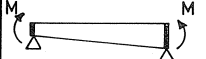
3.5 *Computer program employed*
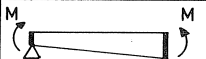
The computer calculations were performed with the aid of the finite element program of Marc Analysis Research Corporation. With this program, called Marc, the magnitude of the load at which loss of stability takes place can be calculated for a structure consisting of an anisotropic material subjected to any loading. The output for this problem consists of a factor by which the actual load must be multiplied in order to attain the critical state and of the eigenvector associated with this.

Before a start was made with the stability calculations for the portal frame, various test calculations were carried out in order to find out to what extent the critical loads calculated with the Marc program are reliable. After some imperfections had been eliminated it was found that the critical loads obtained with Marc are in very good agreement with values calculated with the aid of analytical methods (see Table 1).

3.6 *Choice of element configuration and element type used*

The element configuration used for all the portal frames, together with the boundary conditions and the loading, is indicated in Fig. 5. For the wind bracing the boundary conditions and element configuration are indicated in Fig. 6.

Tabel 1. Test results of the Marc computer program

Test results.		Dimension in mm.					
	length	height	width.	material	analytical	Marc	deviation
	2000	200	10	timber	Pk = 113.1 N	Pk = 109 N	3.5 %
	2000	200	10	steel	Pk = 2159 N	Pk = 2182 N	1.0 %
	4000	200	20	timber	Pk = 148 N Pk = 166 N	Pk = 150 N Pk = 170.5 N	1.3 % 2.7 %
	4000	200	20	steel	Pk = 8535 N Pk = 8886 N	Pk = 8824 N Pk = 9079 N	2.1 % 3.3 %
	4000	200 500	20	timber	Mk = 804 Nm Mk = -804 Nm	Mk = 786 Nm Mk = -788 Nm	2.2 % 2.0 %
	4000	200 500	20	steel	Mk = 44.65 kNm Mk = -44.65 kNm	Mk = 45 kNm Mk = -45 kNm	0.8 % 0.8 %

8
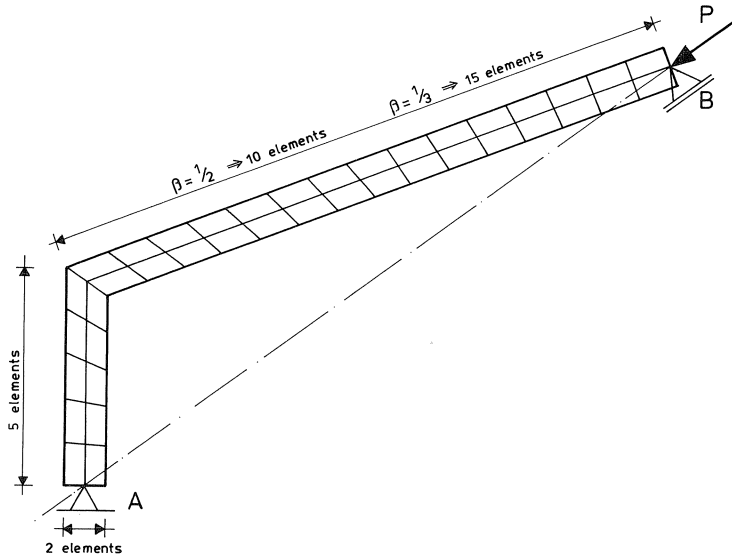
Fig. 5.   Element configuration adopted for the frame.
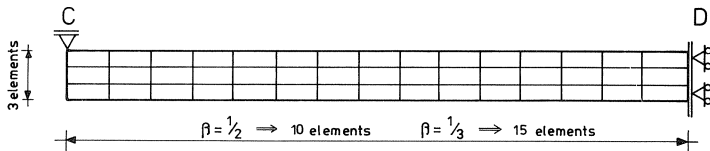
Fig. 6.   Element configuration adopted for the wind bracing.

The type of element adopted is a "bilinear thick shell element" with four corner nodes and six degrees of freedom per node. As the machine time for stability calculations with Marc very greatly increases when the number of degrees of freedom per element becomes larger, this type of element with a relatively small number of degrees of freedom is very suitable for calculations of this kind. A disadvantage is that with this approach the compatibility requirements can be satisfied only at a limited number of points of the element. This being so, the element does indeed correctly describe the behaviour of the structure on average, but a stress analysis may reveal that at some integration points the stress may well deviate somewhat from the expected value.

3.7   *Material properties introduced*

Although the differential equations comprise, in accordance with the beam theory, only one modulus of elasticity and one shear modulus, more material data are needed for the computer calculations. The computer establishes for the chosen type of element a stiffness matrix which, for the type chosen for the present purpose, is as follows:

$$
\begin{bmatrix} \varepsilon_{xx} \\ \varepsilon_{yy} \\ \varepsilon_{zz} \\ \gamma_{xy} \\ \gamma_{yz} \\ \gamma_{zx} \end{bmatrix} = \begin{bmatrix} 1 \cdot /E_{xx} & -v_{yx}/E_{yy} & -v_{zx}/E_{zz} & 0 & 0 & 0 \\ -v_{xy}/E_{xx} & 1 \cdot /E_{yy} & -v_{zy}/E_{zz} & 0 & 0 & 0 \\ -v_{xz}/E_{xx} & -v_{yz}/E_{yy} & 1 \cdot /E_{zz} & 0 & 0 & 0 \\ 0 & 0 & 0 & 1 \cdot /G_{xy} & 0 & 0 \\ 0 & 0 & 0 & 0 & 1 \cdot /G_{yz} & 0 \\ 0 & 0 & 0 & 0 & 0 & 1 \cdot /G_{zx} \end{bmatrix} \begin{bmatrix} \sigma_{xx} \\ \sigma_{yy} \\ \sigma_{zz} \\ \sigma_{xy} \\ \sigma_{yz} \\ \sigma_{zx} \end{bmatrix}
$$

Since the analysis is based on a symmetric stiffness matrix, the following values must be input into the computer:

$$E_{xx},\ E_{yy},\ E_{zz},\ v_{xy},\ v_{yz},\ v_{zx},\ G_{xy},\ G_{yz} \text{ and } G_{zx}$$

With laminated timber, as considered here, there is no question of a definite wood grain (fibre) direction for the structure as a whole. Apart from the axial direction, the orientation of the fibres may differ greatly from one ply to another (see Fig. 7).
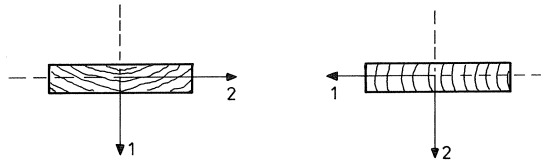
Fig. 7.   Possible fibre orientation in the plies.

This means that in timber frames of laminated construction there occurs an averaging of the various stiffness properties in the plane perpendicular to the fibre direction.

For the purpose of the present stability analysis the actual stiffness properties of laminated wood were not investigated in detail. As the basic material of the frames considered in this research was in most cases softwood (deal), the following values were input into the computer:

$E_{xx} = 11000 \text{ N/mm}^2$
$E_{yy} = E_{zz} = 600 \text{ N/mm}^2$
$v_{xy} = 0{,}48$
$v_{yz} = 0{,}45$
$v_{zx} = 0{,}036$
$G_{zy} = 500 \text{ N/mm}^2$
$G_{yz} = 200 \text{ N/mm}^2$
$G_{zx} = 500 \text{ N/mm}^2$

In making this choice of values the wood was assumed to have a moisture content of approximately 12%, and a local co-ordinate system for the orientation of the fibres as shown in Fig. 8 was adopted.

10
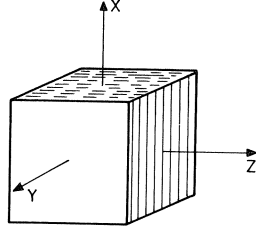
Fig. 8. Orientation of wood fibres.

3.8 *Set-up of computer calculation; results*

In order to let the results of the calculation cover the widest possible range the differential equations (1) to (4) have been rearranged as nondimensional expressions (see Appendix B). With the approximation that I_p for narrow rectangular sections can be taken as equal to $bh^3/12$ and using the abbreviations indicated below, the differential equations for the roof beam can be written as:

$$\theta = z/L; \quad \xi = u/L; \quad \varkappa = EI_w/EI_y; \quad k = \frac{PL^2}{EI_y}; \quad \frac{GI_t}{EI_y} = 0{,}182; \quad \frac{h}{L} = S; \quad \frac{EC_w}{L^2 EI_y} = \tfrac{1}{12}S^2 \quad (5)$$

$$(1 + \varkappa)\xi^{\text{xxxx}} + \tfrac{1}{2}\varkappa S\varphi^{\text{xxxx}} + k \cos v\xi^{\text{xx}} - k \sin v \cdot \theta \cdot \varphi^{\text{xx}} - 2k \sin v \cdot \varphi^{\text{x}} = 0 \quad (6)$$

$$\left(\tfrac{1}{3} + \varkappa\right) \cdot \tfrac{1}{4}S^2 \cdot \varphi^{\text{xxxx}} + \tfrac{1}{2}S\varkappa\xi^{\text{xxxx}} - 0{,}182\varphi^{\text{xx}} + k \cos v\tfrac{1}{12}S\varphi^{\text{xx}} - k \sin v\theta\xi^{\text{xx}} = 0 \quad (7)$$

(x denote derivatives with respect to θ)

With the aid of these abbreviations the differential equations for the column can likewise be rewritten in nondimensional form, except that now an extra factor, namely β, is introduced because of the difference in length between the column and the roof beam:

$$\xi^{\text{xxxx}} + k \cdot \beta^2 \cdot \sin \gamma\xi^{\text{xx}} - k \cdot \beta^2 \cos \gamma\theta\varphi^{\text{xx}} - 2k \cdot \beta^2 \cos \gamma \cdot \varphi^{\text{x}} = 0 \quad (8)$$

$$\frac{1}{12\beta^2} \cdot S^2 \cdot \varphi^{\text{xxxx}} - 0{,}182\varphi^{\text{xx}} + k\beta^2 \sin \gamma \cdot \frac{1}{12\beta^2} \cdot S^2 \cdot \varphi^{\text{xx}} - k\beta^2 \cos \gamma\theta\xi^{\text{xx}} = 0 \quad (9)$$

The k-value (PL^2/EI_y) of the frame is what we are really interested in. With the aid of equations (5) to (9) it becomes apparent that this k-value is governed mainly by the following quantities:
- χ: the ratio EI_w/EI_y
- S: the ratio h/L
- β: the ratio of column length to beam length
- α: the slope of the roof

With the aid of the above considerations it was determined how the computer calculations could best be set up. Frames with a column/beam length ratio β of $1:2$ and $1:3$ were investigated, for roof slope angles α of 10°, 20° and 30°, for values of $S(= h/L)$ of $1:14$, $1:11$ and $1:8$, and for values of χ $(= EI_w/EI_y)$ of 50, 100 and ∞. It should be noted

11

that for $\chi = 50$ and $\chi = 100$ only the extreme values of S were considered, namely, $1:14$ and $1:8$.

As the finite element method uses absolute values, not ratios or relative values, the above-mentioned parameters were applied with $L = 8000$ mm and $L = 12000$ mm and with $b = 100$ mm.

At the start of this research it was suspected that the stiffness of wind bracings as employed in practice is so great that portal frames behave rather in the manner of structures with infinitely rigid lateral restraint of the upper edge. If proved correct, this supposition would mean that the effect of the bracing could, for the purpose of the further investigation of the problem, be confined to assuming a fully restrained upper edge, which would constitute a major simplification. Accordingly, this aspect was first investigated. In [12] the stiffness of wind bracings is considered with reference to a pratical test. If the results obtained in that research are "translated" into values applicable to three-hinged portal frames, it appears that in practice the ratio EI_w/EI_y for these structures is approximately in the range from 100 to 400. For this reason it was decided, besides analysing frames with infinitely rigid lateral support for the upper edge, to analyse frames with EI_w/EI_y equal to 50 and to 100.

Before the results of the calculations are presented, the convergence criterion applied by Marc will first be explained. This will enable the differences between the various critical loads to be better assessed.

The eigenvalues of the stiffness matrix that has been established are calculated by Marc with the aid of an iteration process in which, per operation, two eigenvalues are calculated, both of which converge, in different ways, to the exact value.

If curves were drawn through points representing these calculated values in a diagram, two different curves would be obtained, both converging, in their respective different ways, to the same value. The iteration process is stopped when the difference between the two values is smaller than a certain predetermined value, the so-called convergence criterion.

A drawback is that this criterion leads to an accurate approximation of the exact value only if the two curves converge in manifestly different ways. If they converge as shown in Fig. 9A, they enclose that exact value between them, in which case the criterion yields accurate results. But if the curves converge in the manner shown in Fig. 9B, the criterion may yield results which deviate more from the exact value then might be supposed.
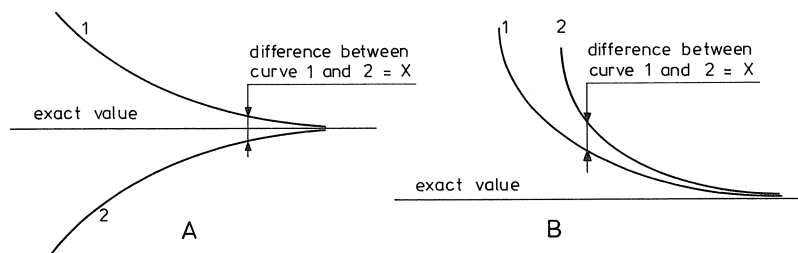
Fig. 9.   Different types of convergence in the iteration process.

12

Unfortunately, in the iteration method used by Marc both of these alternative "convergence processes", as represented in the respective diagrams, may occur. In the present research this has been allowed for by adopting a smaller value for the convergence criterion (namely, 0,1%) in a case corresponding to Fig. 9B than in a case corresponding to Fig. 9A (for which a value of 1% is adopted). This considerably improves the situation, but deviations of $\pm 1\%$ between the critical loads – due to the above-mentioned phenomena – nevertheless remain.

The critical loads calculated with the aid of the computer are given in Table 2. As appears from Table 2, there is very little difference in the critical load for frames with $\chi = 100$ and $\chi = \infty$ respectively. The maximum deviation that occurs is only 4%. The eigenvectors for these frames also differ very little. The eigenvector for a frame with $\chi = 100$ is shown in Fig. 10, from which it is apparent that the displacements of the bracing are negligible in relation to the lateral displacements of the frame.

The deviations revealed by the calculations should be viewed in the context of the accuracy of other assumptions made in analysing this kind of frames. For the type of portal frame and loading under investigation it then appears permissible to draw the following conclusion:

"Half frame units which form part of a three-hinged gable-type roof frame and are

Table 2. Results of calculations

α	β	S	P_k in kN for $\chi = \infty$	for $\chi = 50$	deviation	P_k in kN for $\chi = 100$	deviation
10°	1/2	1/14	96,5	93,7	2,9%	95,1	1,5%
10°	1/2	1/11	115,3				
10°	1/2	1/8	135,95	132,4	2,6%	134,15	1,3%
20°	1/2	1/14	95,1	92,7	2,5%	94	1,2%
20°	1/2	1/11	113,3				
20°	1/2	1/8	134	130,65	2,5%	132,5	1,1%
30°	1/2	1/14	95,7	93,4	2,4%	94,5	1,3%
30°	1/2	1/11	113,4				
30°	1/2	1/8	133,5	131,25	1,7%	132,75	0,6%
10°	1/3	1/14	112,2	103	8,1%	107,7	4%
10°	1/3	1/11	119,7				
10°	1/3	1/8	129,4	125,5	3%	127,75	1,3%
20°	1/3	1/14	110	102,2	7,1%	106	3,6%
20°	1/3	1/11	118,05				
20°	1/3	1/8	130,2	125	4%	127	2,5%
30°	1/3	1/14	108,5	103,25	4,8%	106,5	1,8%
30°	1/3	1/11	118,15				
30°	1/3	1/8	127,9	124	3%	126,1	1,4%

α = slope of roof beam
β = length of column/length of roof beam
S = depth of cross-section/length of roof beam
χ = flexural stiffness of bracing/lateral stiffness of frame $(= EI_w/EI_y)$

supported along the upper edge of the roof beam by a wind bracing of such stiffness that $EI_w/EI_y \geqslant 100$ will show the same theoretical twist-bend buckling behaviour as such units in which the upper edge has infinitely rigid support against lateral displacement".

For practical purposes this means that for the normal three-hinged portal frame structures the two halves thereof can, in so far as their theoretical twist-bend stability is concerned, be conceived as infinitely rigidly supported along the upper edge.

In view of the above conclusion, the further investigation was confined to studying the twist-bend buckling behaviour of frames with infinitely rigid lateral support for the upper edge.
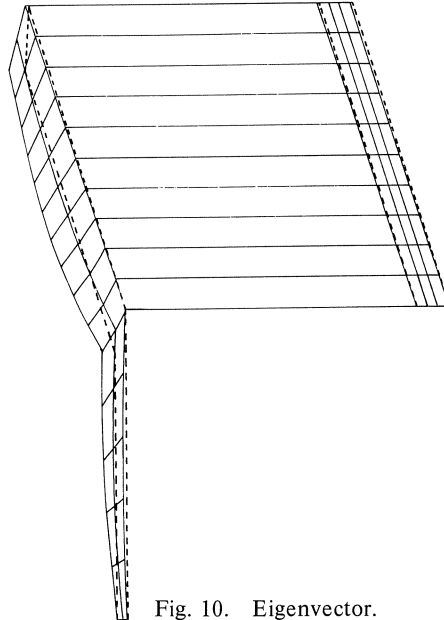
Fig. 10.   Eigenvector.

3.9   *Twist-bend buckling behaviour of portal frames with infinitely rigidly supported upper edge*

With the aid of the values given in Table 2, the values of k for the frames analysed with $\chi = \infty$ are listed in Table 3.

The negative bending moment which occurs at the knee of the frame is equal to:

$$M_{kr} = P_k \cdot \beta L \cos \gamma \tag{10}$$

Multiplying both sides of the equation $P_k = k \cdot EI_y/L^2$ by $\beta L \cos \gamma$, we can write:

$$M_{kr} = \mu \frac{EI_y \cdot \beta}{L} \tag{11}$$

14

$$\mu = k \cos \gamma \tag{12}$$

The values of μ are also given in Table 3.

Besides k and μ, this table contains the maximum compressive stresses occurring in the roof beam at the knee of the frame. From these figures it appears that for a large proportion of the frames under investigation the flexural stress at which instability develops is below the failure stress of wood. For deal the failure stress is approximately 30 N/mm^2.

By plotting the calculated values of k and μ in a graph it is fairly easy to estimate the k or μ of a structure with parameter values which are intermediate between those investigated.

For the values of μ these graphs are presented in Fig. 11.

As already stated, the computer program supplies, besides the critical loads of the structures, also the associated eigenvectors. The way in which the vectors are represented in this report calls for some clarification.

An overall x-y-z co-ordinate system has been adopted, in which the x-y plane coincides with the plane of the portal frame. As the nodal displacements in the x-y plane are negligible in relation to the displacements in the z-direction, only the latter have been plotted in the diagrams. The displacements in the z-direction have been plotted in the x-y plane and more particularly in relation to the outer edge of the unloaded frame. The lines 1, 2 and 3 represent the displacements in the z-direction of the inner edge, the centre-line and the outer edge respectively. The distance between line 1 and the outer edge of the unloaded frame is therefore a measure of the displacement of the inner edge
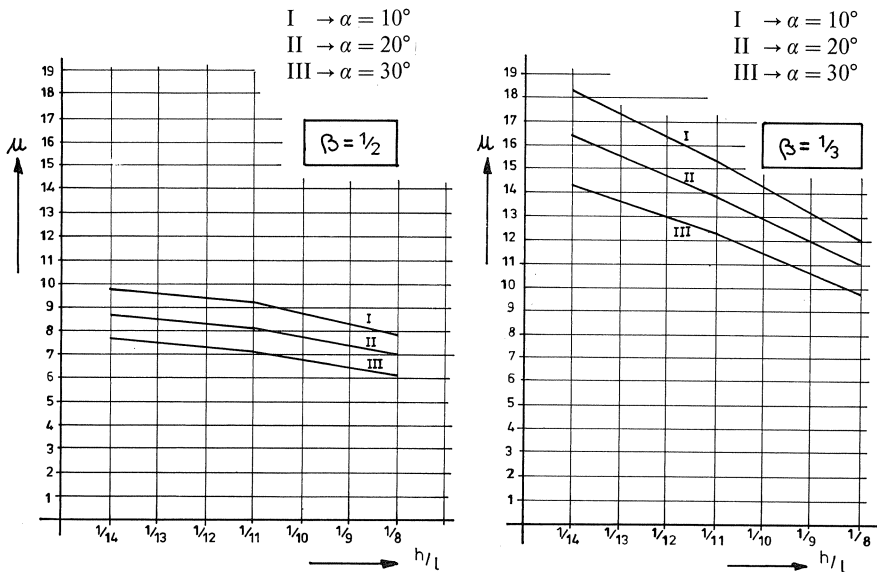

Fig. 11. Values of μ.

15

in the z-direction. By way of illustration, two characteristic eigenvectors are shown in Figs. 12 and 13. For the other eigenvectors see Appendix 3.

Table 3.   Results of calculations for frames with infinitely rigid lateral support along the upper edge

α	β	S	P_{kr} in kN for $\chi = \infty$	k	M_{kr} in kN for $\chi = \infty$	μ	σ_{kr} in N/mm^2
10°	1/2	1/14	96,5	11,78	318,55	9,72	60,0
10°	1/2	1/11	115,3	11,06	380,6	9,13	44,5
10°	1/2	1/8	135,95	9,49	448,77	7,83	28,2
20°	1/2	1/14	95,1	11,6	283,3	8,64	53,5
20°	1/2	1/11	113,3	10,87	337,52	8,10	39,7
20°	1/2	1/8	134	9,35	399,19	6,96	25,2
30°	1/2	1/14	95,7	11,68	250,64	7,65	47,5
30°	1/2	1/11	113,4	10,87	297,0	7,12	35,1
30°	1/2	1/8	133,5	9,32	349,64	6,10	22,2
10°	1/3	1/14	112,2	20,54	399,1	18,26	33,8
10°	1/3	1/11	119,7	17,25	425,77	15,34	22,6
10°	1/3	1/8	129,4	13,55	460,27	12,05	13,1
20°	1/3	1/14	110	20,14	357,28	16,36	30,4
20°	1/3	1/11	118,05	17,01	383,43	13,81	20,4
20°	1/3	1/8	130,2	13,63	422,89	11,07	12,1
30°	1/3	1/14	108,5	19,86	312,7	14,31	26,7
30°	1/3	1/11	118,15	17,02	340,51	12,26	18,2
30°	1/3	1/8	127,9	13,39	368,61	9,65	10,7

α = slope of roof beam
β = length of column/length of roof beam
S = depth of cross-section/length of roof beam
$\chi = EI_w/EI_y$
$k = P_{kr} \cdot L^2/EI_y$
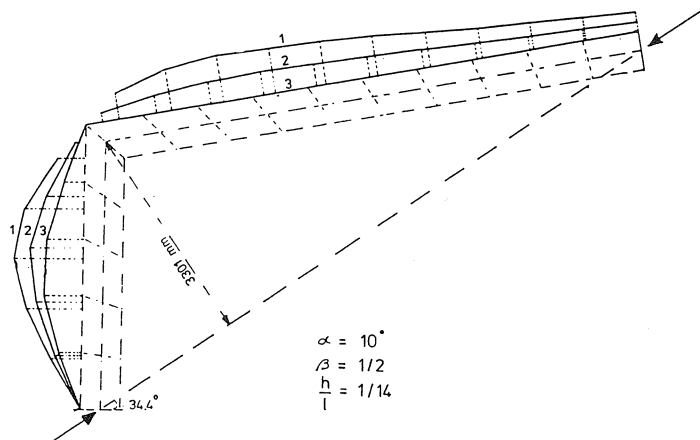$\mu = M_{kr} \cdot L/EI_y \cdot \beta$
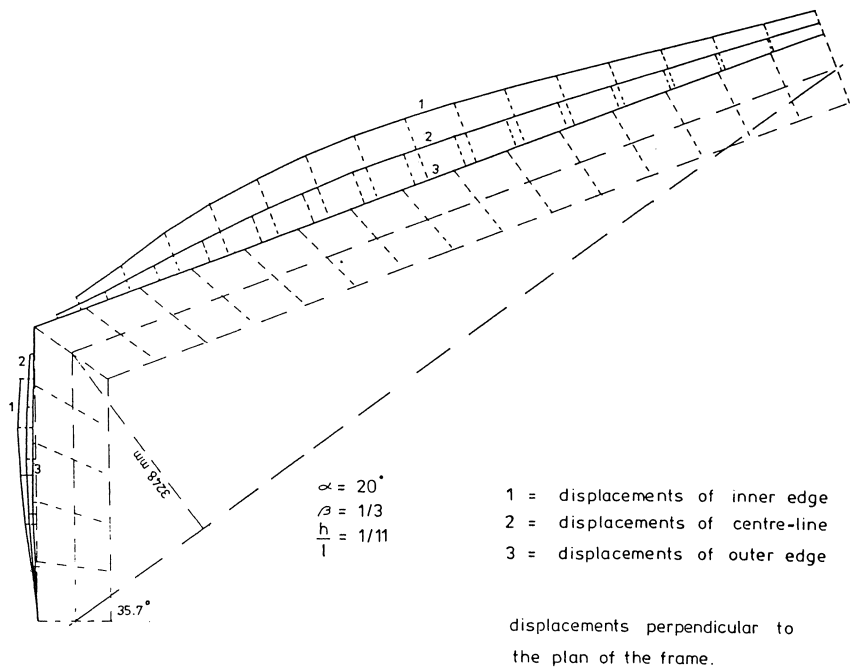

Fig. 12.   Eigenvector.

16

α = 20°
β = 1/3
h/l = 1/11

32.48 mm

35.7°

1 = displacements of inner edge
2 = displacements of centre-line
3 = displacements of outer edge

displacements perpendicular to
the plan of the frame.

Fig. 13. Eigenvector.

3.10 *Interpretation of the eigenvectors*

It appears that, besides some transitional forms, two fundamentaly different types of eigenvector are to be distinguished. Representatives of both types are shown in Figs. 12 and 13. In the case of Fig. 12 the column undergoes very large displacements indeed so large that the maximum nodal displacement of the vector occurs at the column. On the other hand, in the case of Fig. 13 the column undergoes hardly any displacement, while mainly the roof beam undergoes displacement in the z-direction. These different forms suggest that loss of stability in some frames is caused by the development of instability of the column and in others by the development of instability of the roof beam. In order to gain more insight into these matters, it was investigated, with the aid of some calculations, which part of the frame is mainly responsible for loss of stability. For this purpose the half frame under consideration was divided into two parts, namely the column and the beam. By introducing some additional boundary conditions we thus obtain two structural members for which it is possible to establish a formula with which the critical load can be calculated (see Fig. 14).

The critical load of the schematized column is approximated by the formula:

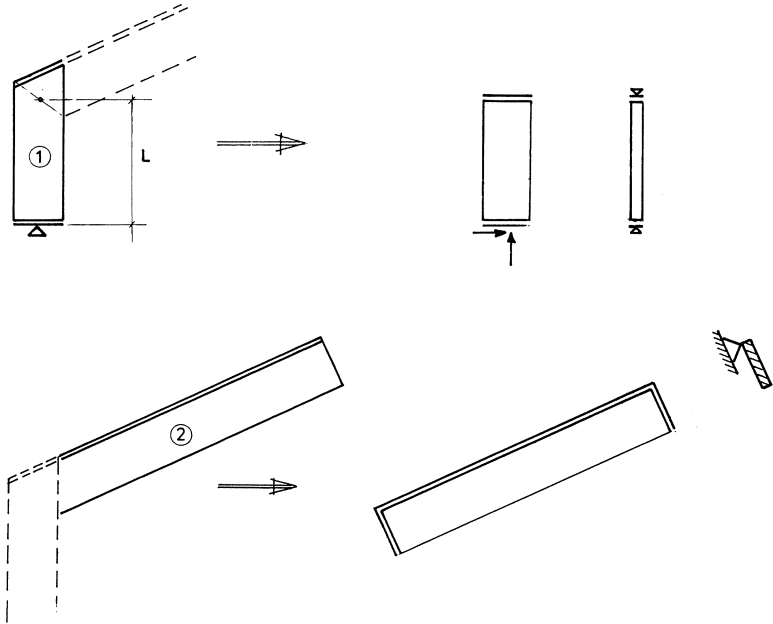$$\frac{N}{N_{kr}} + \frac{M}{M_{kr}} \leqslant 1 \qquad (13)$$

17

Fig. 14.   Schematized column and roof beam.

where:

$$N = P \sin \gamma, \quad M = P \cos \gamma L\beta, \quad N_{kr} = \frac{\pi^2 EI_y}{(L\beta)^2} \quad \text{en} \quad M_{kr} = 1{,}75 \frac{\pi}{\beta L} \sqrt{EI_y \cdot GI_t} \qquad (14)$$

Formula (13) can now be written as follows:

$$P_{kr} \leqslant \left(\frac{\sin \gamma}{N_{kr}} + \frac{\beta L \cos \gamma}{M_{kr}} \right)^{-1} \qquad (15)$$

The critical loads calculated with the aid of this formula are given in Table 4.

Because it is difficult to find for a roof beam a formula which provides a reasonably good approximation of the critical load, a different approach was adopted for this member.

Since the beam can be conceived as infinitely rigidly supported along its upper edge, the differential equations (1) and (2) can be transformed with the aid of

$$U_{\text{bracing}} = \tfrac{1}{2} h \times \varphi \qquad (16)$$

into the following differential equation (see Appendix 4):

$$(EI_y \cdot \tfrac{1}{4} h^2 + EC_w) \varphi'''' + (-GI_t + \tfrac{1}{3} h^2 N + hM) \varphi'' = 0 \qquad (17)$$

This differential equation is not directly soluble for the roof beam of the portal frame with its specific boundary conditions. The beam has therefore been conceived as a variant of the basic case as represented in Fig. 15.
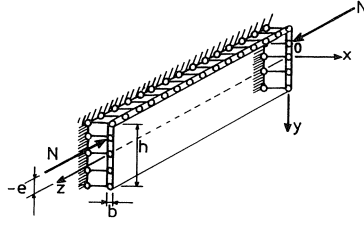
18

Fig. 15.   Schematized roof beam.

The following expression can be derived for the critical load of this structure (see Appendix D):

$$N_{kr} = \frac{EI_y}{L^2} \frac{\left(\pi^2 + \dfrac{12G}{ES^2}\right)}{\left(1 + \dfrac{3e}{h}\right)} \qquad (18)$$

where $S = h/L$

The roof beam of the portal frame differs from this basic case in three respects:
- The roof beam is loaded by a linearly varying moment.
- At the roller bearing at the top of the frame the angular rotation is not restrained.
- At the knee of the frame the roof beam is partly restrained, i.e., there is partial fixity.

Because of these differences the critical load of the roof beam will differ from the basic case. For the roof beam the critical load can, for example, be written as follows (see Appendix D):

$$P \cos v = \frac{EI_y}{L^2} \cdot \frac{\left(\pi^2 + \dfrac{12G}{ES^2}\right)}{\left(1 + \dfrac{3 \sin v}{S}\right)} * \delta \qquad (19)$$

(δ is a correction factor which need not necessarily be constant)

From research on the twist-bend buckling behaviour of straight beams it is known that the critical load of a beam subjected to a bending moment configuration differing from the basic case can nevertheless be calculated with the formula for the basic case, provided that the critical value is multiplied by a factor f. This factor will depend on the shape of the bending moment diagram [18].

   In [18] it is also shown that different boundary conditions can quite suitably be taken into account by replacing the actual length of the structure by an effective length.

   Since the bending moment configuration for all the frames investigated differs in the same way from the basic case, it can be assumed that f is the same for all these frames. The absence of the fork at the roller bearing likewise occurs in all the frames, and therefore the effective length will, for all the roof beams, increase by very nearly equal

19

amounts in consequence of this. The effect of the partial fixity differs from one frame to another, but these differences are bound to be minimal for frames with the same roof slope and same β.

In view of the above considerations the factor δ will vary only slightly for roof beams with the same slope and same β. For those frames in which loss of stability is caused mainly by the development of instability in the roof beam the factor δ will therefore have to be substantially equal for frames having the same α and β. The values of δ have been calculated for all the frames under investigation and are listed in table 4.

It appears from Table 4 that in all the frames with $\beta = \frac{1}{3}$ the loss of stability is caused mainly by the development of instability of the roof beam. In the case of frames with $\beta = \frac{1}{2}$ there sometimes occurs instability of the column and sometimes a form of stability loss in which both the column and the beam play a major part.

When further research throws more light on how the column and the roof beam of the portal frame influence each other, it should be possible to establish formulae and/or graphs with which an effective length can be determined for both members. It will then very probably be possible to calculate the critical load fairly accurately with the aid of these effective lengths and formulae (15) and (19).

Table 4.   Results of calculations for the schematized frame members

α	β	S	P_k in kN for $\chi = \infty$	P_k in kN of the schematized column	P_k in kN of the schematized roof beam	δ
10°	1/2	1/14	96,5	80,1	57,4	1,68
10°	1/2	1/11	115,3	102,0	59,4	1,94
10°	1/2	1/8	135,95	139,9	64,4	2,11
20°	1/2	1/14	95,1	85,0	62,1	1,53
20°	1/2	1/11	113,3	108,2	64	1,77
20°	1/2	1/8	134	148,7	69,4	1,93
30°	1/2	1/14	95,7	92,1	68,8	1,39
30°	1/2	1/11	113,4	117,2	70,9	1,60
30°	1/2	1/8	133,5	161	76,7	1,74
10°	1/3	1/14	112,2	115,5	49,6	2,26
10°	1/3	1/11	119,7	146,7	51,1	2,34
10°	1/3	1/8	129,4	201,9	54,6	2,37
20°	1/3	1/14	110	121,2	53,6	2,05
20°	1/3	1/11	118,05	154	55,1	2,14
20°	1/3	1/8	130,2	211,9	59,7	2,18
30°	1/3	1/14	108,5	130,2	59,3	1,83
30°	1/3	1/11	118,15	165,4	60,9	1,94
30°	1/3	1/8	127,9	227,6	65,3	1,96

α = slope of roof beam
β = length of column/length of roof beam
S = depth of cross-section/length of roof beam
$\chi = EI_w/EI_y$
δ = correction factor

Although the results of the calculations for the frames investigated here do not point in that direction, it will be necessary to devote more attention to the form of stability loss in which both the column and the roof beam play a major part. The reason is that under loading conditions which cause the column and the beam to become unstable simultaneously there is the danger that the critical load will be considerably reduced, for then the restraining effect that these members have upon each other will no longer exist.

4 Arch frames

4.1 *Frames investigated*

Arch frames occur in various forms in constructional practice. For example, a distinction may be drawn between circular, parabolic and sinusoidal arches. They may be used as three-hinged or as two-hinged frames (see Fig. 16).

As it was not possible to investigate all these types of arch frame, a choice had to be made. The doctoral thesis by E. Katzschner [17] played an important role in making this choice. In his thesis, entitled "Ein Beitrag zum Verformungs- und Kipp-problem des kreisförmig gekrümmten Stabes" ("A contribution on the deformation and twist-bend buckling behaviour of the circular-curved bar"), Katzschener shows that it is possible to derive an analytical solution for the critical load on laterally restrained arch frames which satisfy certain conditions. These conditions are:

a. The frames must have a constant radius of curvature (circular shape) and a constant single symmetric cross-section.

b. The frames must be laterally supported along the whole length of the arch. Such support may be applied at any point within the depth of the curved beam, but the location of that point must be constant all along the arch.

c. The stiffness of this lateral support must be so great that the arch can, at this support, be regarded as rigidly restrained.

d. The loading must consist of a tensile or a compressive force acting along the chord of the frame.

e. The arch frames must be provided with fork-type bearings at their ends.

On comparing these conditions with the inferences drawn from the analysis of the twist-bend buckling behaviour of gable-type portal frames laterally supported by bracings it
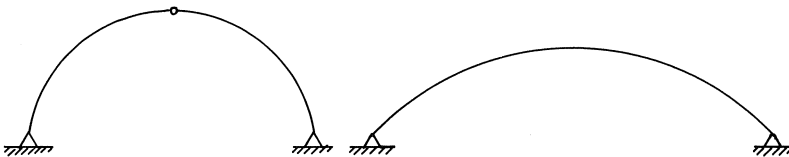
Fig. 16.   Three-hinged and two hinged arch frame.

21

can reasonably be expected that in practice condition (c) will be satisfied in most cases.

With regard to conditions (d) and (e) it can be stated that condition (d) is very suitable for investigating the twist-bend buckling behaviour of arch members forming part of a three-hinged frame, but that such frames will in practice usually not satisfy condition (e).

In the case of two-hinged arch frames the situation is reversed: they usually satisfy condition (e), but in this case condition (d) is not representative of the critical twist-bend buckling load in practice.

As for condition (b), it is to be noted that it is satisfied in a great many cases in practice.

So it appears that the twist-bend buckling behaviour of an arch frame which satisfies the above-mentioned conditions is not entirely representative of the theoretical behaviour of the circular arch structures shown in Fig. 16.

It is, however, not unusual to assume that arch frames such as those employed in constructional practice can be regarded as variants of a basic case. This basic case could be the arch frame which satisfies the conditions stated here. From this point of view an analytical solution for the basic case can be of much value in connection with further investigation of the problem. It was for this reason that it was decided that the time available under the present research project for studying the behaviour of arch frames could most advantageously be employed in studying, interpreting and verifying E. Katzschner's research.

In his thesis E. Katzschner, after discussing the geometry of curves, derives the differential equations for an arbitrarily curved bar of single symmetric cross-sectional shape and loaded in an arbitrary manner. Next, with the aid of these general differential equations, he derives the differential equations for the various sub-sets of the set of curved structures under consideration. This is done by imposing more and more restrictions upon the geometry and the loading of the structure. In this way there ultimately remains a structure subjected to a particular load, for which Katzschner is then able to solve the differential equations analytically. The structure to which this case is applicable satisfies the conditions enumerated at the start of this chapter.

Since the manner in which Katzschner derives the differential equations for the arch structures that he ultimately analyses is rather laborious, those equations have here been derived once again, but using a direct approach. This derivation is given for an arch frame of bisymmetric cross-sectional shape, a choice justified by the fact that cross-sections with only one axis of symmetry are seldom used for timber arch structures. The type of arch structure for which this derivation has been established is shown in Fig. 17. With regard to in-plane forces acting on it the structure is provided with a hinge at point A and with a roller bearing – allowing displacement along the chord A-B of the arch – at point B. As for the out-of-plane forces the structure satisfies the above-mentioned conditions (b) to (e).
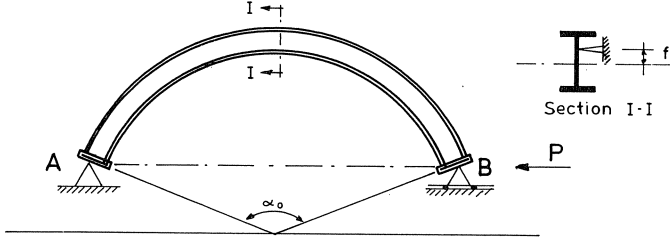
22

Fig. 17. Arch frame investigated.

4.2 Differential equations

The differential equations can be derived with the aid of equilibrium considerations or energy considerations. As in the case of portal frames, the method which uses the calculus of variations and the principle of minimum potential energy was adopted, and the following assumptions were made:

- The structure consists of a homogeneous isotropic material, and the laws of Hooke and Bernoulli are valid.
- The deformations within the plane of the structure are negligibly small.
- The cross-sectional shape does not change during twist-bend buckling.
- The loading does nog change its direction of action.
- The effect of shear deformation and deformation due to axial force is neglected.

In order to have an interim check, the differential equations have initially been derived for a laterally unsupported circular arch frame.

The differential equations are as follows (see Appendix E):

1. $EI_x \left(\dfrac{d^4 V_s}{ds^4} - \dfrac{d^2 \varphi_z}{ds^2} \cdot \dfrac{1}{r} \right) + EC_w \left(\dfrac{d^4 \varphi_z}{ds^4} \cdot \dfrac{1}{r} + \dfrac{d^4 V_s}{ds^4} \cdot \dfrac{1}{r^2} \right) - \dfrac{GI_{t\,red}}{r} \left(\dfrac{d^2 \varphi_z}{ds^2} + \dfrac{d^2 V_s}{ds^2} \cdot \dfrac{1}{r} \right)$

$- \dfrac{d^2 V_s}{ds^2} \left(\dfrac{M_y}{r} - S_z \right) - \dfrac{d^2}{ds^2} (M_y \cdot \varphi_z) + 2 S_x \dfrac{d^2 V_s}{ds^2} \cdot \dfrac{1}{r} - S_z \cdot \varphi_z \cdot \dfrac{1}{r} = 0$ 　　　(20)

2. $EC_w \left(\dfrac{d^4 \varphi_z}{ds^4} + \dfrac{d^4 V_s}{ds^4} \cdot \dfrac{1}{r} \right) - GI_{t\,red} \cdot \left(\dfrac{d^2 \varphi_z}{ds^2} + \dfrac{d^2 V_s}{ds^2} \cdot \dfrac{1}{r} \right) - EI_x \left(\dfrac{d^2 V_s}{ds^2} \cdot \dfrac{1}{r} - \dfrac{\varphi_z}{r^2} \right)$

$- \dfrac{d^2 V_s}{ds^2} M_y + \dfrac{M_y}{r} \cdot \varphi_z = 0 \qquad (GI_{t\,red} = GI_t - S_z \cdot i_p^2)$ 　　　(21)

For the limit case $R \to \infty$ these equations become the differential equations for a laterally unsupported straight beam (see [3] and [4]).

For the laterally supported arch frame shown in Fig. 17 the relation between V_s and φ is approximately expressed by:

$V_s = \varphi_z \times f$ 　　　(22)

23

With the aid of this relation and by making use of polar co-ordinates it is possible to replace the above differential equations by the following differential equation (see Appendix F)

$$\frac{EC_w}{r^2}\,\ddot{\varphi_z}\left(1+\frac{f}{r}\right)^2 - GI_{t\,red}\cdot\ddot{\varphi_z}\left(1+\frac{f}{r}\right)^2 + EI_x\left(\ddot{\varphi_z}\,\frac{f^2}{r^2}-2\cdot\frac{f}{r}\,\ddot{\varphi_z}+\varphi_z\right)-(M_y\cdot\varphi_z)^{\cdot\cdot}\cdot f$$

$$+S_z f^2\ddot{\varphi_z}+2S_x f^2\dot{\varphi_z}-S_z\cdot f\cdot r\cdot\varphi_z-M_y\cdot\ddot{\varphi_z}\,f\left(1+\frac{f}{r}\right)+M_y\cdot r\cdot\varphi_z=0 \qquad (23)$$

Katzschner makes use of Galerkin's method to obtain an approximate solution of this equation. For the structure shown in Fig. 18 this approach leads finally to two expressions for the critical load.

For the critical tensile load:

$$P_k=\frac{\bar{a}_1\cdot4\cdot\dfrac{\pi^4}{\alpha_0^3}+\bar{a}_2\,\dfrac{\pi^2}{\alpha_0}+a_4\,\dfrac{\alpha_0}{4}}{r\left[4f\,\dfrac{\pi^2}{\alpha_0^2}\left(\sin\dfrac{\alpha_0}{2}-\dfrac{1}{2}\,\dfrac{\sin\left(2\pi-\frac{1}{2}\alpha_0\right)}{4\pi/\alpha_0-1}-\dfrac{1}{2}\,\dfrac{\sin\left(2\pi+\frac{1}{2}\alpha_0\right)}{4\pi/\alpha_0+1}-\dfrac{\alpha_0}{2}\cos\dfrac{\alpha_0}{2}\right)\right.}$$

$$+f\,\frac{\pi}{\alpha_0}\left(\frac{\sin\left(2\pi-\frac{1}{2}\alpha_0\right)}{4\pi/\alpha_0-1}-\frac{\sin\left(2\pi+\alpha_0/2\right)}{4\pi/\alpha_0+1}\right)+\frac{r}{2}\left(\sin\frac{\alpha_0}{2}-\right.$$

$$\left.\left.-\frac{1}{2}\,\frac{\sin\left(2\pi-\frac{1}{2}\alpha_0\right)}{4\pi/\alpha_0-1}-\frac{1}{2}\,\frac{\sin\left(2\pi+\frac{1}{2}\alpha_0\right)}{4\pi/\alpha_0+1}\right)-\frac{r}{4}\,\alpha_0\cos\frac{\alpha_0}{2}\right] \qquad (32)$$
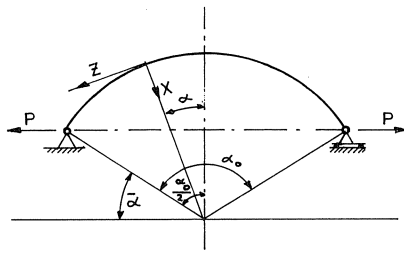
for $\alpha_0=\pi$ this expression can be written as:

$$P_k=\frac{15\pi\left(4\bar{a}_1+\bar{a}_2+\frac{1}{4}a_4\right)}{r(56f+8r)}$$

For the critical compressive load:

$$P_k=\frac{-\left(\bar{a}_1\,\dfrac{\pi^4}{\alpha_0^4}+\bar{a}_2\,\dfrac{\pi^2}{\alpha_0^2}+a_4\right)\alpha_0}{r\left[2f\,\dfrac{\pi^2}{\alpha_0^2}\left(2\sin\dfrac{\alpha_0}{2}+\dfrac{\sin\left(\pi-\frac{1}{2}\alpha_0\right)}{2\pi/\alpha_0-1}+\dfrac{\sin\left(\pi+\frac{1}{2}\alpha_0\right)}{2\pi/\alpha_0+1}-\alpha_0\cos\dfrac{\alpha_0}{2}\right)\right.}$$

$$-2f\,\frac{\pi}{\alpha_0}\left(\frac{\sin\left(\pi-\frac{1}{2}\alpha_0\right)}{2\pi/\alpha_0-1}-\frac{\sin\left(\pi+\alpha_0/2\right)}{2\pi/\alpha_0+1}\right)+r\left(2\sin\frac{\alpha_0}{2}+\right.$$

$$\left.\left.+\frac{\sin\left(\pi-\frac{1}{2}\alpha_0\right)}{2\pi/\alpha_0-1}+\frac{\sin\left(\pi+\frac{1}{2}\alpha_0\right)}{2\pi/\alpha_0+1}\right)-r\alpha_0\cos\frac{\alpha_0}{2}\right] \qquad (34)$$

for $\alpha_0=\pi$ this expression can be written as:

$$P_k=-\frac{3\pi\left(\bar{a}_1+\bar{a}_2+a_4\right)}{8r(f+r)} \qquad (35)$$

24

$$S_{\bar{z}} = -P\cos\alpha \qquad (24)$$
$$S_x = -P\sin\alpha \qquad (25)$$
$$M_y = -P.r.(\cos\alpha - \cos\tfrac{\alpha_0}{2}) \qquad (26)$$
$$N_y = P.r.\sin\alpha \qquad (27)$$
$$M_y = P.r.\cos\alpha \qquad (28)$$

$$\bar{a}_1 = \frac{E\,C_\omega}{r^2} \qquad (29)$$
$$\bar{a}_2 = GI_t \text{ red} \qquad (30)$$
$$a_4 = EI_x \qquad (31)$$

Fig. 18. Schematic of Arch frame investigated.

4.3 Checking the formulae with the Marc computer program

The formulae for the critical twist-bend buckling load presented here are approximate formulae. Their accuracy is largely dependent on the difference between the chosen expression for the behaviour of φ and the actual behaviour. Katzschner assumes that for loading by a compressive force the behaviour of φ can be described by:

$$\varphi_z = b_1 \cos\pi\frac{\alpha}{\alpha_0} \qquad (36)$$

In order to verify this assumption and to obtain some insight into the accuracy of the formulae derived, a number of arch frames were analysed with the Marc finite element program. The results thus obtained, together with the values calculated with the aid of the formulae, are given in Table 5. The eigenvectors associated with these critical loads are shown in Fig. 19.

Table 5. Results of calculations for arch frames

arch nr.	α_0	material	R in mm	h/R	P_{kr} with Marc (P_{Marc})	P_{kr} with formula (P_{form})	$\dfrac{P_{form} - P_{Marc}}{P_{Marc}} \times 100$
1	$\pi/2$	timber*	10000	0,04	4836 N	5898	21,8
2	$\pi/2$	timber*	10000	0,06	7120 N	9274	30,2
3	π	timber*	10000	0,10	11820 N	13434	13,6
4	π	timber*	10000	0,07	8270 N	9258	11,9

* deal softwood with stiffness properties as for portal frames

It appears from Table 5 that the critical loads calculated with Marc differ from those obtained with the approximate formulae. The difference associated with frames subtending a central angle $\alpha_0 = \pi/2$ is almost twice as large as that associated with a central angle $\alpha_0 = \pi$.

These differences are to a great extent explicable with the aid of the eigenvectors. In all four cases the eigenvector is found to deviate from the assumed cosinusoidal shape, a deviation which occurs more particularly near the ends of the arch (see Fig. 19).

Since the "edge disturbance", on account of the length of the arch structure, is of greater influence in frames with $\alpha_0 = \pi/2$ than in those with $\alpha_0 = \pi$, it appears logical

25

that the difference found to exist between "Marc" and "formula" is indeed greater in the former frames.

From the results obtained it emerges that Katzschner's assumption for the behaviour of φ is a very rough approximation. The inclusion of more than one term in the series with which φ is approximated will certainly yield better results.

It can be concluded from the foregoing that the approximate formulae given for the critical twist-bend buckling load of laterally supported arch frames with a chord load are too inaccurate. It can be presumed, however, that with some additional effort it should be possible to derive more accurate formulae which can then provide a suitable basis for further investigation.

In discussing the boundary conditions of the arch frame analysed it was noted that

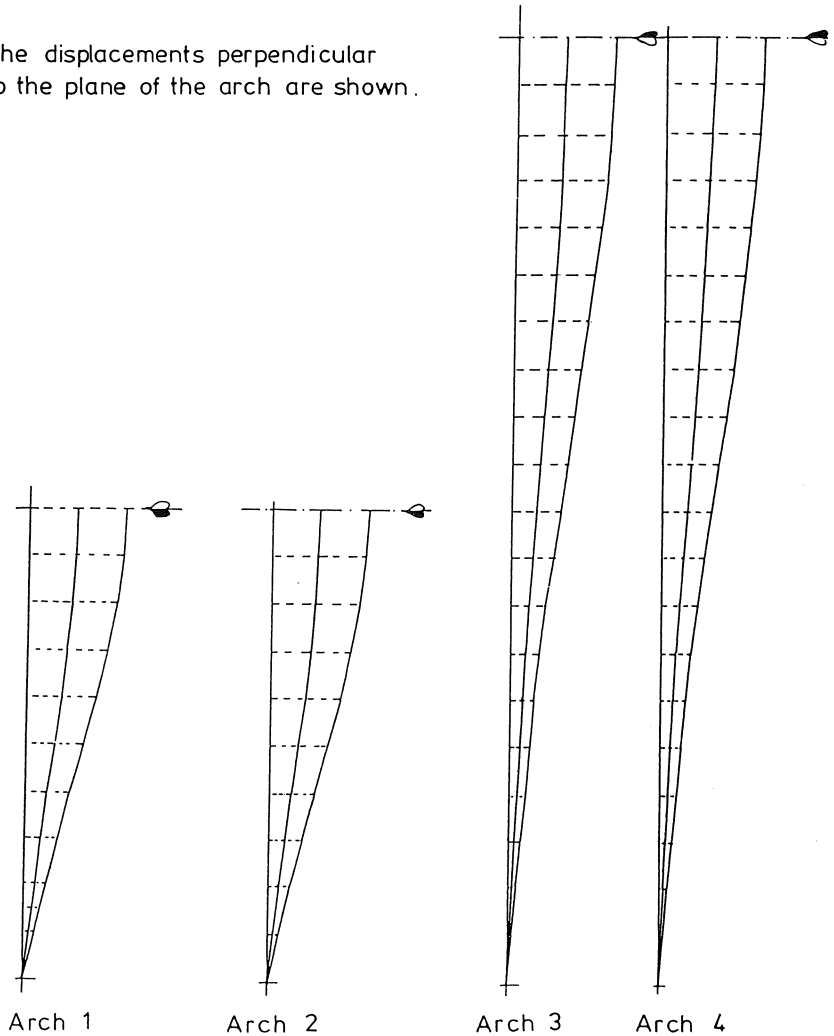The displacements perpendicular
to the plane of the arch are shown.

Arch 1   Arch 2   Arch 3   Arch 4

Fig. 19. Eigenvectors.

26

arch members which form part of a three-hinged frame usually have no fork-type bearing at the top hinge. As it involved little effort to analyse this variant with the aid of the computer, the critical loads and eigenvectors were, for the arch frames with $\alpha_0 = \pi/2$ under consideration, also calculated for the case where the fork-type bearing at the top is absent.

The results obtained are presented here without comment:

arch nr.	α_0	material	R in mm	h/R	P_{kr} calculated with Marc
1	$\pi/2$	timber	10000	0,04	4012 N
2	$\pi/2$	timber	10000	0,06	5965 N

The eigenvectors obtained are respresented in Fig. 20.
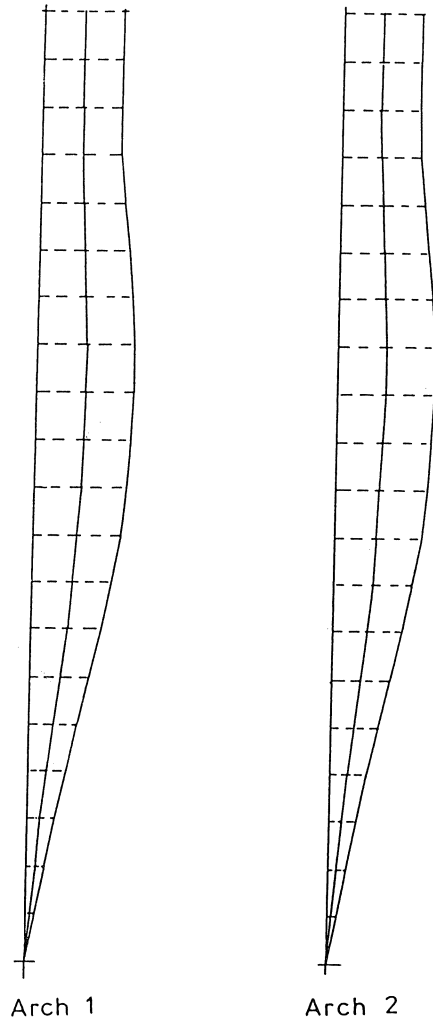

Arch 1   Arch 2

Fig. 20. Eigenvectors.

5 Summary and conclusions

An investigation into the twist-bend buckling (or lateral torsional buckling) behaviour of timber portal frames and arch frames is reported. After the problem has been defined, the lateral (twist-bend) stability of gable-type portal frames, resiliently supported along the upper edge by a wind bracing and subjected to a compressive load acting along the chord of the frame, is first treated. The differential equations are derived. As these are not amenable to solution by manual methods, a computer is used in the further investigation.

With the aid of the results of the calculations for the frames in question it is shown that the twist-bend buckling behaviour of portal frames with a lateral flexural stiffness which is 100 times lower than that of the wind bracing is the same as that of portal frames with rigid lateral support of the upper edge. Furthermore, it appears that the flexural stress at which loss of stability occurs is, for a high proportion of the frames investigated, below the failure stress of the wood. For the frames used in normal constructional practice the flexural stiffness of the bracing is between 150 and 400 times the lateral flexural stiffness of the frames, and for this reason the further investigation concentrates on studying the twist-bend buckling behaviour of portal frames with infinitely rigid lateral support of the upper edge.

This behaviour is studied with the aid of eigenvectors calculated by the computer. These vectors show that in principle there are three ranges of behaviour with regard to the initiation of loss of stability of the frame:
- a range in which the roof beam of the portal frame develops instability;
- a range in which the column of the portal frame develops instability;
- a transitional range.

The first part of the research is concluded with the derivation of formulae with which the behaviour of gable-type portal frames, in the first two above-mentioned ranges, can be calculated with reasonably good approximation.

The second part of this research consists in studying the twist-bend buckling behaviour of circular bisymmetric arch frames, with rigid lateral support, subtending a central angle of any magnitude and loaded in tension or in compression along the chord. After derivation of the differential equations of the laterally unsupported arch frame, the differential equations for the arch frame with rigid lateral support are derived and are solved with the aid of Galerkin's method. This method yields very simple formulae for the critical load. Their accuracy was checked with the aid of a finite element program, which showed that, considering how simple they are, the accuracy of these formulae is tolerably good.

6 Acknowledgements

Structural Engineering of the Eindhoven University of Technology.

The author wishes to take this opportunity to express to all these concerned his thanks for the excellent guidance and advice he received in the course of his studies.

7 Notation

A	cross-sectional area of portal frame
F	cross-sectional area of arch frame
x, y, z	rectangular co-ordinates
b, h	width and depth of cross-section
L	length of roof beam
βL	length of column
$\gamma, \varkappa, \alpha$	angles
E	modulus of elasticity
G	elastic shear modulus
EI_x	flexural stiffness about x-axis
EI_y	flexural stiffness about y-axis
EI_w	flexural stiffness of wind bracing
GI_t	St. Venant torsional stiffness
EC_w	warping stiffness
I_p	polar moment of inertia
S_x, S_y, S_z	axial force in directions x, y, z respectively
N	axial force
N_{kr}	critical axial force
P	concentrated load
P_{kr}	critical concentrated load
M_x, M_y, M_z	moment about axes x, y, z respectively
M_{kr}	critical moment
i_p^2	I_p/A
u, V	displacements
r, R	radius
e	eccentricity of axial force
f	eccentricity of lateral support
φ	angle of twist
ν	Poisson's ratio
ε	axial strain
σ	stress
$\gamma_{xy}, \gamma_{yz}, \gamma_{zx}$	shearing strain components
$\varkappa$	EI_w/EI_y nondimensional parameter
δ	modification factor
S	(portal frames): h/L, nondimensional parameter
s	(arch frames): arc length
U_t	total potential energy
$GI_{t\,r}$	$GI_t - S_z \cdot i_p^2$

8 References

1. TIMOSHENKO, S. P. and J. M. GERE, Theory of elastic stability (2nd ed.).
2. CHEN, W. F. and T. ATSUTA, Theory of beam-columns, Vol. 2.
3. VLASOV, V. Z., Thin-walled elastic beams (2nd ed.).
4. BLEICH, F., Buckling strength of metal structures.
5. BÜRGEMEISTER, G., H. STEUP and H. KRETZSCHMAR, Stabilitätstheorie mit Erläuterungen zu der Knick- und Beulvorschriften (Teil 1 und 2).
6. JOHNSTON, B. G., Guide to stability design criteria for metal structures.
7. Column Research Committee of Japan, Handbook of structural stability.
8. VANDEPITTE, D., Berekening van konstrukties, deel 1 en 2.
9. LOVE, A. E. H., A treatise on the mathematical theory of elasticity.
10. SOLKOLNIKOFF, I. S., Mathematical theory of elasticity.
11. BLAAUWENDRAAD, J. and A. W. M. KOK, Elementenmethode voor constructeurs, deel 2.
12. BRUENINGHOFF, H., Spannungen und Stabilität bei quergestützten Brettschichtträgern.
13. HEMPEL, G., Freigespannte Holzbinder.
14. Delft University of Technology, Lecture Notes No. 103230 K2, Inleiding tot de stabiliteit van het evenwicht.
15. Delft University of Technology, Lecture Notes No. g72.I 304590, Ontwerp en dimensionering van boogspanten.
16. Delft University of Technology, Lecture Notes No. g50/52/53/K.1, Hout en houtconstructies.
17. KATZSCHNER, E., Ein Beitrag zur Verformungs- und Kipp-Problem des kreisförmig gekrümmten Stabes.
18. NETHERCOT, A. A. and N. S. TRAHAIR, Lateral buckling approximations for elastic beams, The Structural Engineer, June 1976, No. 6, Vol. 54.

30

APPENDIX A

Differential equations for the portal frame

$$\gamma = \arctan \frac{\beta + \sin \alpha}{\cos \alpha} \quad (A-1)$$

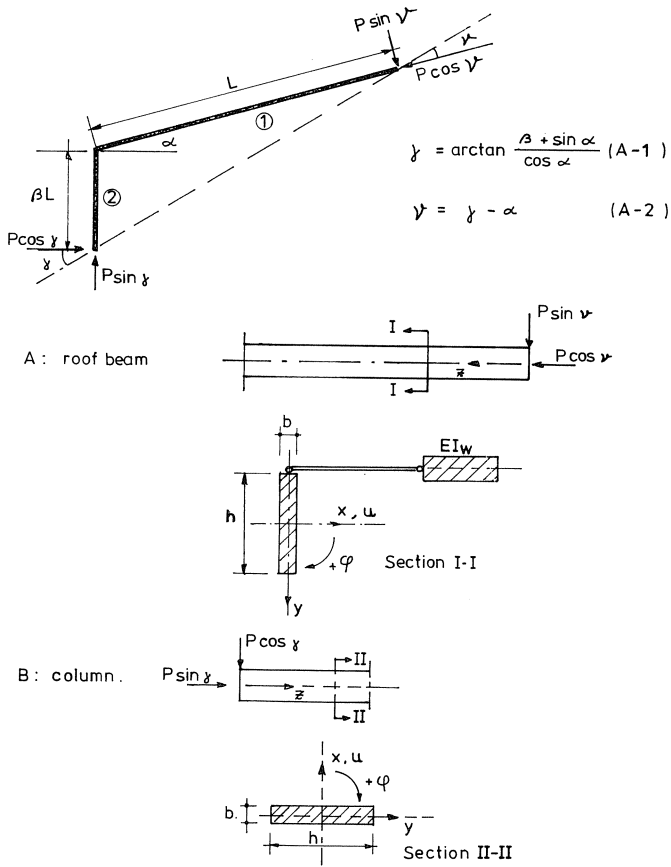$$\nu = \gamma - \alpha \quad (A-2)$$

Fig. 21. Schematic diagram of the frame investigated.

The differential equations are derived with the aid of the calculus of variations and the principle of minimum potential energy.

Roof beam:
The elastic energy during twist-bend buckling is:

$$E_a = \tfrac{1}{2}EI_y \int_0^1 \left(\frac{d^2u}{dz^2}\right)^2 \, dz + \tfrac{1}{2}GI_t \int_0^1 \left(\frac{d\varphi}{dz}\right)^2 \, dz + \tfrac{1}{2}EC_w \int_0^1 \left(\frac{d^2\varphi}{dz^2}\right)^2 \, dz$$

$$+ \tfrac{1}{2}EI_w \int_0^1 \left(\frac{d^2\left(u + \tfrac{1}{2}h\varphi\right)}{dz^2}\right)^2 \, dz \tag{A3}$$

31

The external work done during twist-bending buckling is:

$$A_a = \tfrac{1}{2}P\cos v \int_0^1 \left(\frac{du}{dz}\right)^2 dz + \tfrac{1}{2}P\cos v \frac{I_p}{A}\int_0^1 \left(\frac{d\varphi}{dz}\right)^2 dz - \int_0^1 M_x\left(\frac{d^2u}{dz^2}\right)\cdot \varphi \cdot dz \qquad (A4)$$

The potential energy is $U_t = E_a - A_a$

$$U_t = \int_0^1 \left(\tfrac{1}{2}EI_y u''^2 + \tfrac{1}{2}GI_t\varphi'^2 + \tfrac{1}{2}EC_w\varphi''^2 + \tfrac{1}{2}EI_w(u'' + \tfrac{1}{2}h\varphi'')^2 - \tfrac{1}{2}P\cos v u'^2\right.$$

$$\left. - \tfrac{1}{2}P\cos v \frac{I_p}{A}\varphi'^2 + M_x\cdot u''\cdot\varphi\right)dz \qquad (A5)$$

The requirement that must be fulfilled for the critical conditions is: $\delta(U_t) = 0$

To fulfil this requirement, the calculus of variations yields the following conditions:

$$\frac{\partial(U_t)}{\partial p} - \frac{d}{dz}\left[\frac{\partial(U_t)}{\partial p'}\right] + \frac{d^2}{dz^2}\left[\frac{\partial(U_t)}{\partial p''}\right] = 0 \qquad (A6)$$

and

$$\left[\frac{\partial(U_t)}{\partial p''}\delta p' - \left\{\frac{d}{dz}\left[\frac{\partial(U_t)}{\partial p''} - \frac{\partial(U_t)}{\partial p'}\right]\right\}\delta p\right]_0^L = 0 \qquad (A7)$$

On differentiation of U_t (equation A5) the equations (A6) and (A7) lead to the following differential equations and boundary conditions:

1. $EI_y u'''' + EI_w(u'''' + \tfrac{1}{2}h\varphi'''') + (M_x\cdot\varphi)'' + P\cos v\cdot u'' = 0 \qquad (A8)$

2. $EC_w\varphi'''' + EI_w(u'''' + \tfrac{1}{2}h\varphi'''')\tfrac{1}{2}h - GI_t\cdot\varphi'' + P\cos v \frac{I_p}{A}\varphi'' + M_x u'' = 0 \qquad (A9)$

Boundary conditions:

$$[EI_y u'' + EI_w(u'' + \tfrac{1}{2}h\varphi'') + M_x\varphi]\delta u'\Big|_0^L -$$

$$[EI_y u''' + EI_w(u''' + \tfrac{1}{2}h\varphi''') + (M_x\varphi)' + P\cos v\cdot u']\delta u\Big|_0^L = 0 \qquad (A10)$$

$$[EC_w\varphi'' + EI_w(u'' + \tfrac{1}{2}h\varphi'')\tfrac{1}{2}h]\delta\varphi'\Big|_0^L -$$

$$\left[EC_w\varphi''' + EI_w(u''' + \tfrac{1}{2}h\varphi''')\tfrac{1}{2}h - GI_t\varphi' + P\cos v \frac{I_p}{A}\varphi'\right]\delta\varphi\Big|_0^L = 0 \qquad (A11)$$

Column:
The differential equations of the column can be derived with the aid of the following relations from equations (A8) to (A11):

$$EI_w = 0, \qquad P\cos v \Rightarrow P\sin\gamma, \qquad L \Rightarrow \beta L \qquad (A12)$$

Differential equations for column:

1. $EI_y u'''' + (M_x \varphi)'' + P \sin \gamma u'' = 0$ (A13)

2. $EC_w \varphi'''' - GI_t \varphi'' + P \sin \gamma \dfrac{I_p}{A} \varphi'' + M_x u'' = 0$ (A14)

Boundary conditions:

$$[EI_y u'' + M_x \varphi]\delta u' \Big|_0^{\beta L} - \left[EI_y u''' + (M_x \cdot \varphi)' + P \sin \gamma u'\right] \delta u \Big|_0^{\beta L} = 0 \qquad \text{(A15)}$$

$$[EC_w \varphi'']\delta \varphi' \Big|_0^{\beta L} - \left[EC_w \varphi''' - GI_t \varphi' + P \sin \gamma \dfrac{I_p}{A} \varphi'\right] \delta \varphi \Big|_0^{\beta L} = 0 \qquad \text{(A16)}$$

33

APPENDIX B

Transforming the differential equations of the portal frame into nondimensional expressions

The following differential equations are valid for the roof beam:

1. $EI_y u'''' + EI_w \left(u'''' + \frac{1}{2}h\varphi''''\right) + \left(M_x \cdot \varphi\right)'' + P\cos v \cdot u'' = 0$ (B1)

2. $EC_w \varphi'''' + EI_w \left(u'''' + \frac{1}{2}h\varphi''''\right)\frac{1}{2}h - GI_t \cdot \varphi'' + P\cos v \frac{I_p}{A} \varphi'' + M_x u'' = 0$ (B2)

With the aid of

$$M_x = -P\sin v \cdot z$$ (B3)

these equations can be written as:

1. $\left(EI_y + EI_w\right)u'''' + EI_w \cdot \frac{1}{2}h \cdot \varphi'''' + P\cos v \cdot u'' - P\sin v \cdot z \cdot \varphi'' - 2P\sin v \cdot \varphi' = 0$ (B4)

2. $\left(EC_w + EI_w \cdot \frac{1}{4}h^2\right)\varphi'''' + \frac{1}{2}h \cdot EI_w u'''' - GI_t \varphi'' + P\cos v \frac{I_p}{A} \varphi'' - P\sin v \cdot z \cdot u'' = 0$ (B5)

Put

$$z = \theta \cdot L \quad \text{and} \quad u = \xi \cdot L \Rightarrow \mathrm{d}z = Ld\theta \quad \text{and} \quad \mathrm{d}u = Ld\xi$$ (B6)

$$
\begin{aligned}
u' &= \frac{\mathrm{d}\xi}{\mathrm{d}\theta} & \varphi' &= \frac{1}{L}\frac{\mathrm{d}\varphi}{\mathrm{d}\theta} \\[2mm]
u'' &= \frac{1}{L}\frac{d^2\xi}{\mathrm{d}\theta^2} & \varphi'' &= \frac{1}{L^2}\frac{d^2\varphi}{\mathrm{d}\theta^2} \\[2mm]
u''' &= \frac{1}{L^2}\frac{d^3\xi}{\mathrm{d}\theta^3} & \varphi''' &= \frac{1}{L^3}\frac{d^3\varphi}{\mathrm{d}\theta^3} \\[2mm]
u'''' &= \frac{1}{L^3}\frac{d^4\xi}{\mathrm{d}\theta^4} & \varphi'''' &= \frac{1}{L^4}\frac{d^4\varphi}{\mathrm{d}\theta^4}
\end{aligned}
$$ (B7)

With the aid of the above expressions equations (B4) and (B5) can be written as follows (* denotes derivative with respect to θ):

1. $\left(EI_y + EI_w\right)\frac{1}{L^3} \xi^{****} + EI_w \cdot \frac{1}{2}h \cdot \frac{1}{L^4} \cdot \varphi^{****} + P\cos v \cdot \frac{1}{L} \cdot \xi^{**} - P\sin v \cdot L \cdot \theta \cdot \frac{1}{L^2} \cdot \varphi^{**} -$

$\qquad - 2P\sin v \cdot \frac{1}{L} \cdot \varphi^{*} = 0$ (B8)

2. $\left(EC_w + EI_w \cdot \frac{1}{4}h^2\right) \cdot \frac{1}{L^4} \cdot \varphi^{****} + \frac{1}{2}hEI_w \cdot \frac{1}{L^3} \cdot \xi^{****} - GI_t \cdot \frac{1}{L^2} \cdot \varphi^{**} + P\cos v \frac{I_p}{A} \cdot \frac{1}{L^2} \cdot \varphi^{**} -$

$\qquad - P\sin v \cdot \theta \cdot L \cdot \frac{1}{L} \cdot \xi^{**} = 0$ (B9)

The following nondimensional constants will now be introduced:

$$\frac{EI_w}{EI_y} = \varkappa; \quad k = \frac{P \cdot L^2}{EI_y}; \quad \frac{GI_t}{EI_y} = 0.182; \quad \frac{h}{L} = S \quad \text{and} \quad \frac{EC_w}{L^2 \cdot EI_y} = \tfrac{1}{12}S^2 \qquad \text{(B10)}$$

After multiplying by L^3/EI_y we can write equation (B8) as:

$$(1 + \varkappa) \cdot \xi^{****} + \tfrac{1}{2}\varkappa s \cdot \varphi^{****} + k \cos v \xi^{**} - k \sin v \cdot \theta \cdot \varphi^{**} - 2k \sin v \cdot \varphi^* = 0 \qquad \text{(B11)}$$

For narrow rectangular cross-sections we may take I_p as being approximately equal to $bh^3/12$. With this value, and after multiplying by L^2/EI_y, equation (B9) can be written as:

$$\left(\tfrac{1}{3} + \varkappa\right) \cdot \tfrac{1}{4}S^2 \cdot \varphi^{****} + \tfrac{1}{2} \cdot S \cdot \varkappa \cdot \xi^{****} - 0.182\varphi^{**} + k \cos v \tfrac{1}{12}S^2 \varphi^{**} - k \sin v \cdot \theta \cdot \xi^{**} = 0 \qquad \text{(B12)}$$

The differential equations (B1) and (B2) can therefore be replaced by the following non-dimensional expressions:

1. $(1 + \varkappa)\xi^{****} + \tfrac{1}{2}\varkappa S \varphi^{****} + k \cos v \xi^{**} - k \sin v \cdot \theta \cdot \varphi^{**} - 2k \sin v \cdot \varphi^* = 0 \qquad \text{(B13)}$

2. $\left(\tfrac{1}{3} + \varkappa\right) \cdot \tfrac{1}{4}S^2 \varphi^{****} + \tfrac{1}{2}S\varkappa \xi^{****} - 0.182\varphi^{**} + k \cos v \tfrac{1}{12}S^2 \varphi^{**} - k \sin v \theta \xi^{**} = 0 \quad \text{(B14)}$

The following differential equations are valid for the column of the portal frame:

1. $EI_y u'''' + (M_x \varphi)'' + P \sin \gamma u'' = 0 \qquad \text{(B15)}$

2. $EC_w \varphi'''' - GI_t \varphi'' + P \sin \gamma \dfrac{I_p}{A} \varphi'' + M_x u'' = 0 \qquad \text{(B16)}$

With the aid of $M_x = -P \cos \gamma \cdot z$ these equations can be written as:

1. $EI_y u'''' + P \sin \gamma u'' - P \cos \gamma z \varphi'' - 2P \cos \gamma \varphi' = 0 \qquad \text{(B17)}$

2. $EC_w \varphi'''' - GI_t \varphi'' + P \sin \gamma \dfrac{I_p}{A} \varphi'' - P \cos \gamma z u'' = 0 \qquad \text{(B18)}$

The length of the columns is βL. Put

$$z = \theta \cdot \beta L \quad \text{and} \quad u = \xi \cdot \theta L \Rightarrow dz = \beta L \, d\theta \quad \text{and} \quad du = \beta L \, d\xi \qquad \text{(B19)}$$
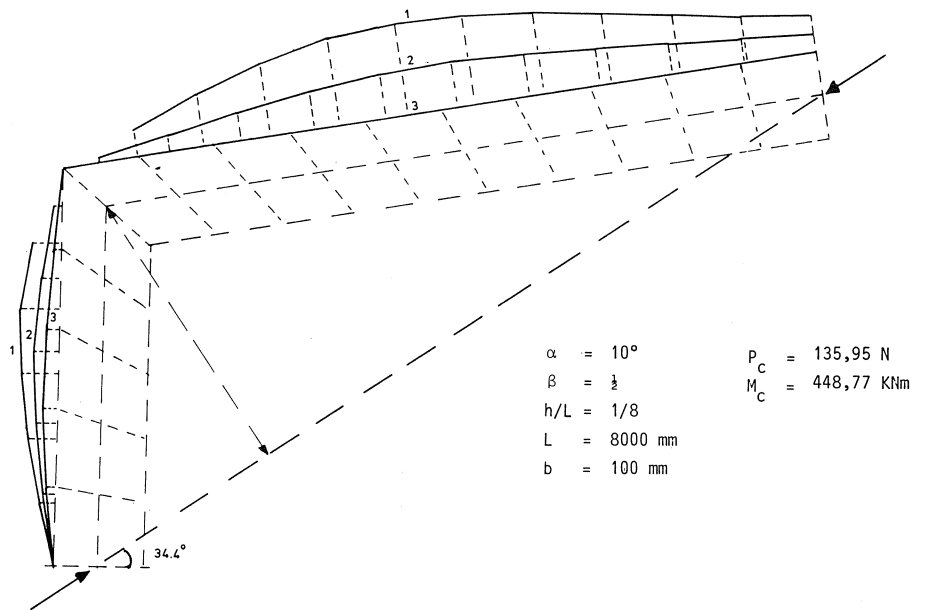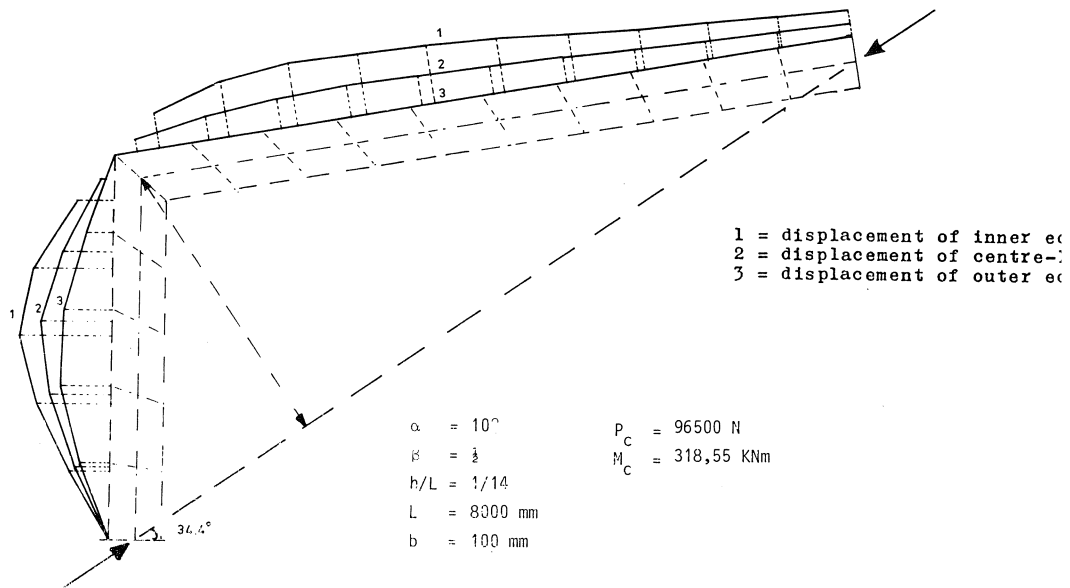
With the aid of the abbreviations introduced for the roof beam it is possible to replace equations (B15) and (B16) by the following nondimensional expressions (these can be derived in the same way as those for the roof beam):
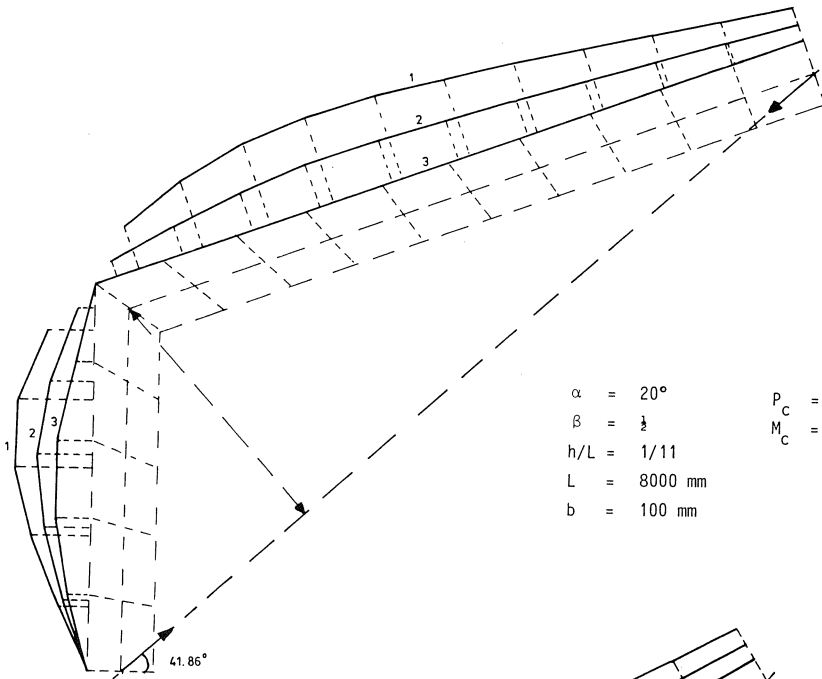
1. $\xi^{****} + k\beta^2 \sin \gamma \xi^{**} - k \cdot \beta^2 \cdot \cos \gamma \cdot \theta \cdot \varphi^{**} - 2k\beta^2 \cos \gamma \varphi^* = 0 \qquad \text{(B20)}$

2. $\dfrac{1}{12\beta^2} \cdot S^2 \cdot \varphi^{****} - 0.182\varphi^{**} + k\beta^2 \sin \gamma \cdot \dfrac{1}{12\beta^2} S^2 \varphi^{**} - k\beta^2 \cos \gamma \cdot \theta \cdot \xi^{**} = 0 \quad \text{(B21)}$
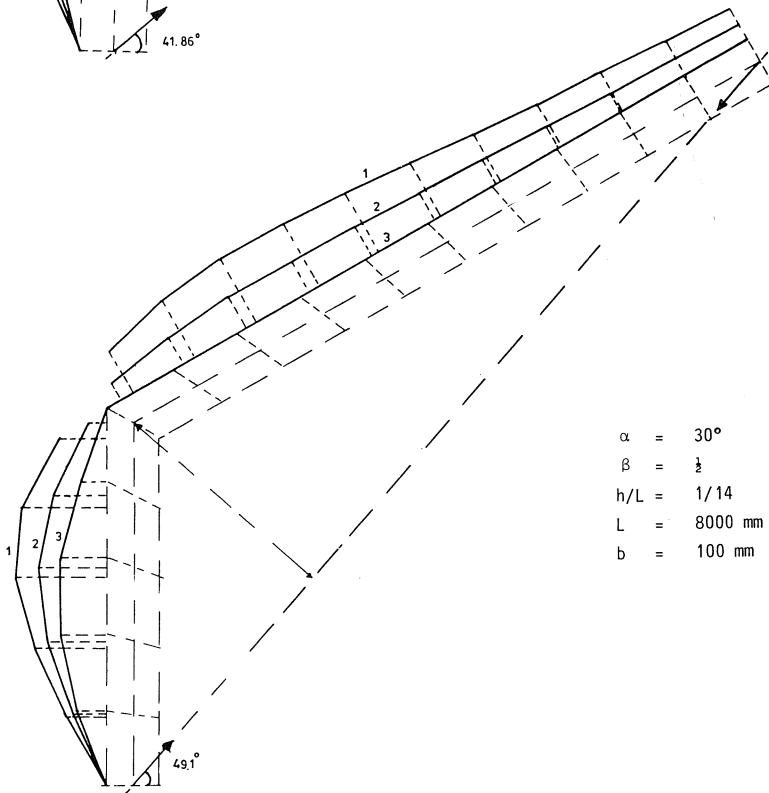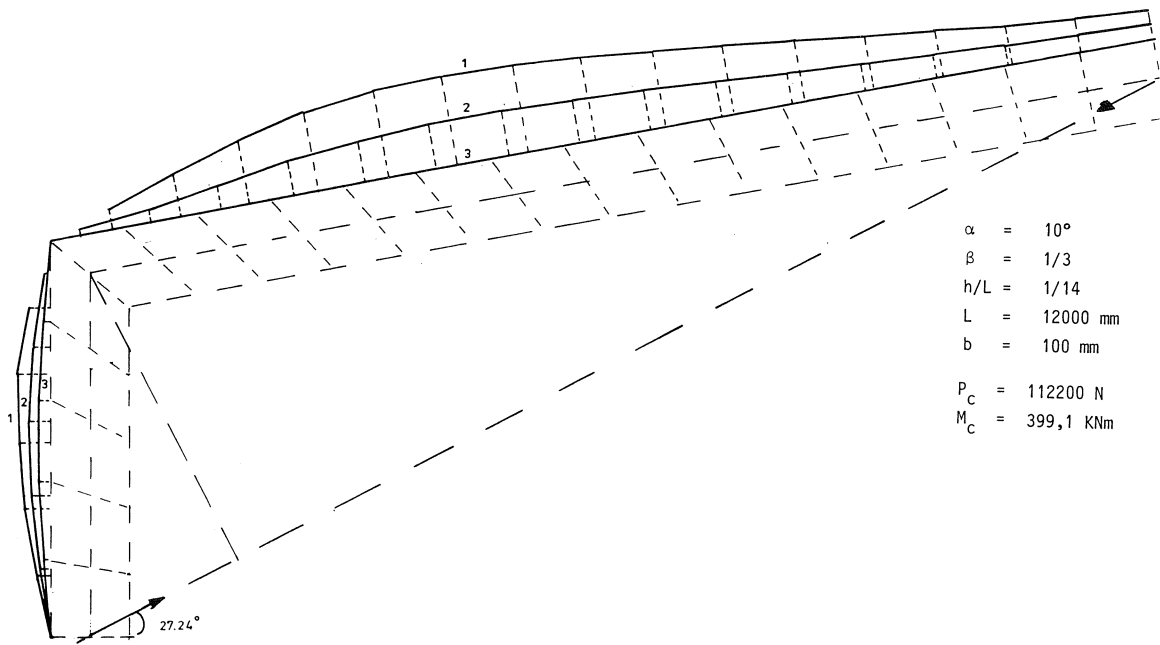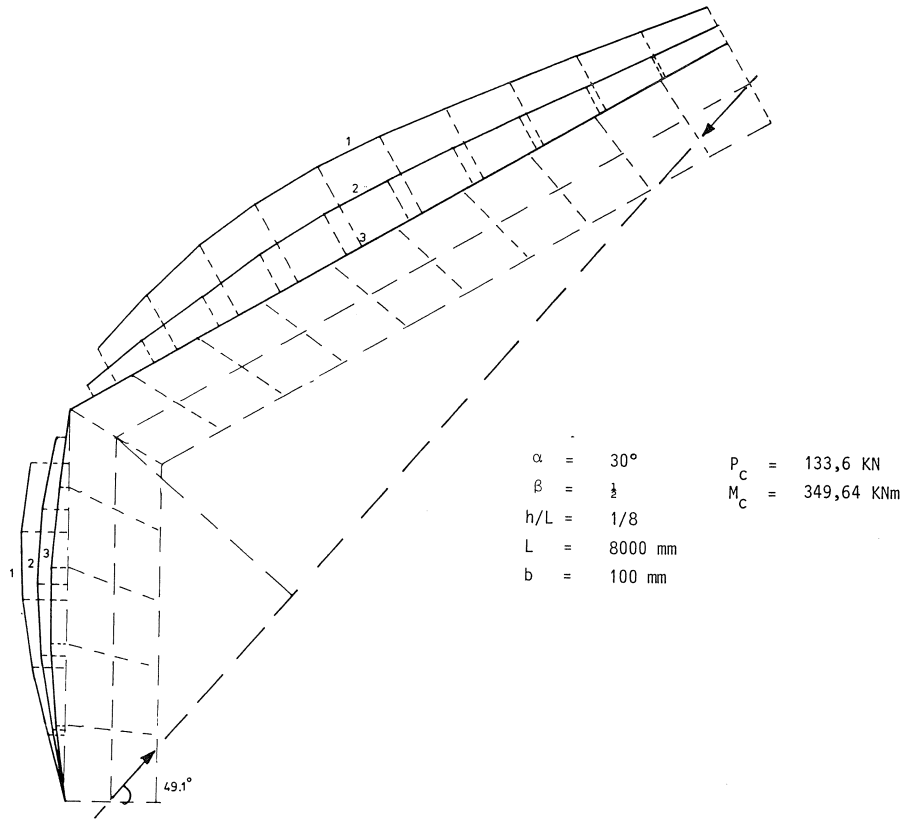
APPENDIX C

Eigenvectors

1 = displacement of inner ed
2 = displacement of centre-l
3 = displacement of outer ed

α = 10° P_c = 96500 N

β = ½ M_c = 318,55 KNm

h/L = 1/14

L = 8000 mm

b = 100 mm

α = 10° P_c = 135,95 N

β = ½ M_c = 448,77 KNm

h/L = 1/8

L = 8000 mm

b = 100 mm

α = 20° P_C = 113300 N
β = ½ M_C = 337,52 N
h/L = 1/11
L = 8000 mm
b = 100 mm

41.86°

α = 30° P_C = 95700 N
β = ½ M_C = 250,64 KNm
h/L = 1/14
L = 8000 mm
b = 100 mm

49,1°

$$\alpha = 30°$$
$$\beta = \tfrac{1}{2}$$
$$h/L = 1/8$$
$$L = 8000 \text{ mm}$$
$$b = 100 \text{ mm}$$

$$P_C = 133,6 \text{ KN}$$
$$M_C = 349,64 \text{ KNm}$$

49.1°

$$\alpha = 10°$$
$$\beta = 1/3$$
$$h/L = 1/14$$
$$L = 12000 \text{ mm}$$
$$b = 100 \text{ mm}$$

$$P_C = 112200 \text{ N}$$
$$M_C = 399,1 \text{ KNm}$$

27.24°

38
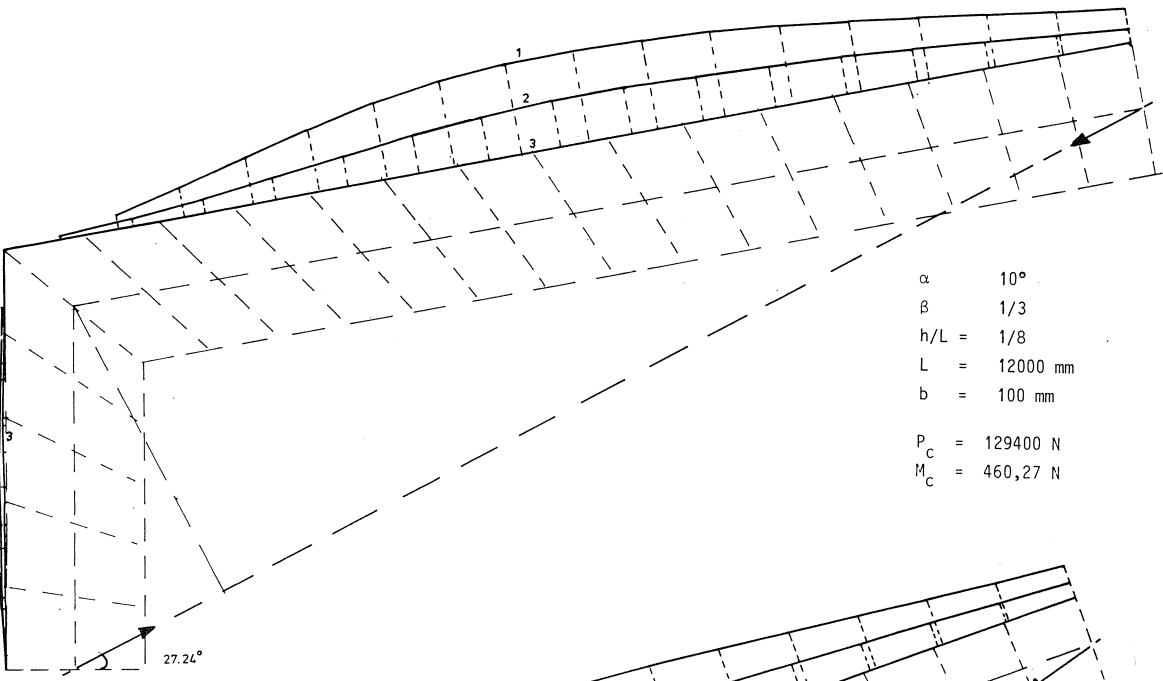
$$\alpha \qquad 10°$$
$$\beta \qquad 1/3$$
$$h/L = \quad 1/8$$
$$L \quad = \quad 12000 \ mm$$
$$b \quad = \quad 100 \ mm$$

$$P_C \quad = \quad 129400 \ N$$
$$M_C \quad = \quad 460,27 \ N$$

27.24°
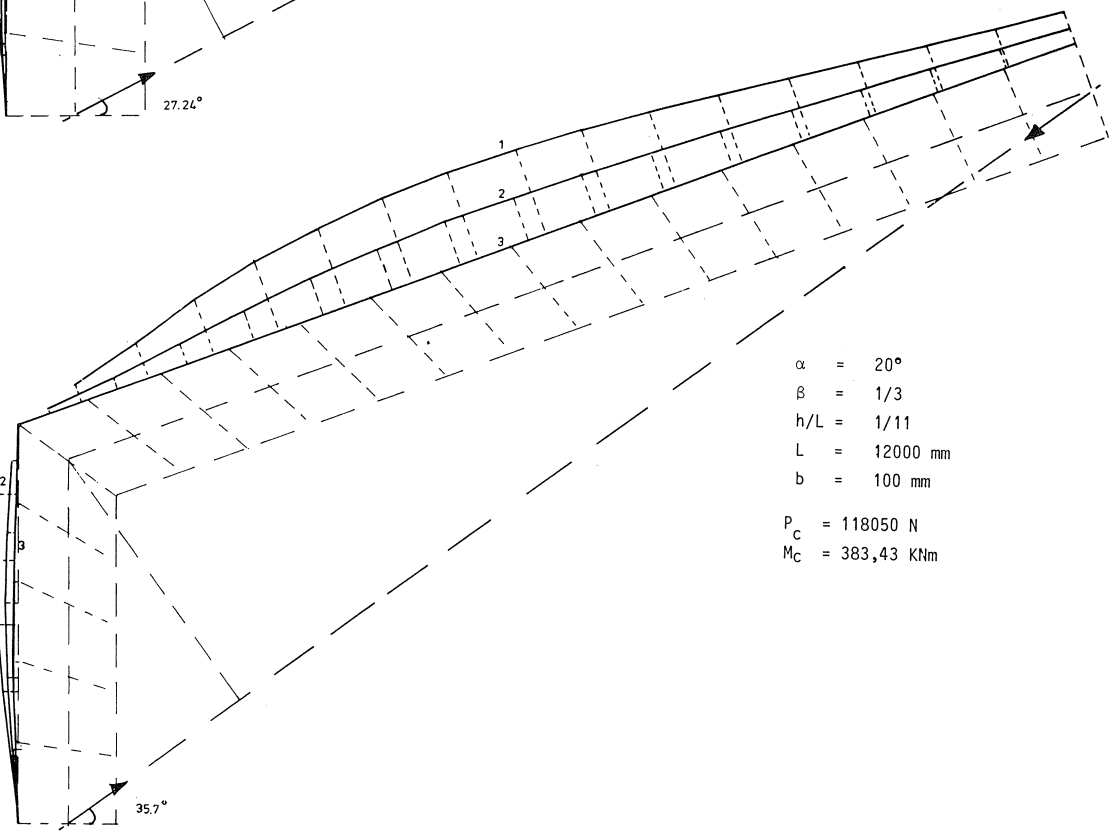
$$\alpha \quad = \quad 20°$$
$$\beta \quad = \quad 1/3$$
$$h/L = \quad 1/11$$
$$L \quad = \quad 12000 \ mm$$
$$b \quad = \quad 100 \ mm$$

$$P_C \quad = \quad 118050 \ N$$
$$M_C \quad = \quad 383,43 \ KNm$$

35.7°

39

$$\alpha = 30°$$
$$\beta = 1/3$$
$$h/L = 1/14$$
$$L = 12000 \text{ mm}$$
$$b = 100 \text{ mm}$$

$$P_c = 108500 \text{ N}$$
$$M_c = 312,7 \text{ KNm}$$

43.9°

$$\alpha = 30°$$
$$\beta = 1/3$$
$$h/L = 1/8$$
$$L = 12000 \text{ mm}$$
$$b = 100 \text{ mm}$$

$$P_c = 127900 \text{ N}$$
$$M_c = 368,61 \text{ KNm}$$

43.9°

40
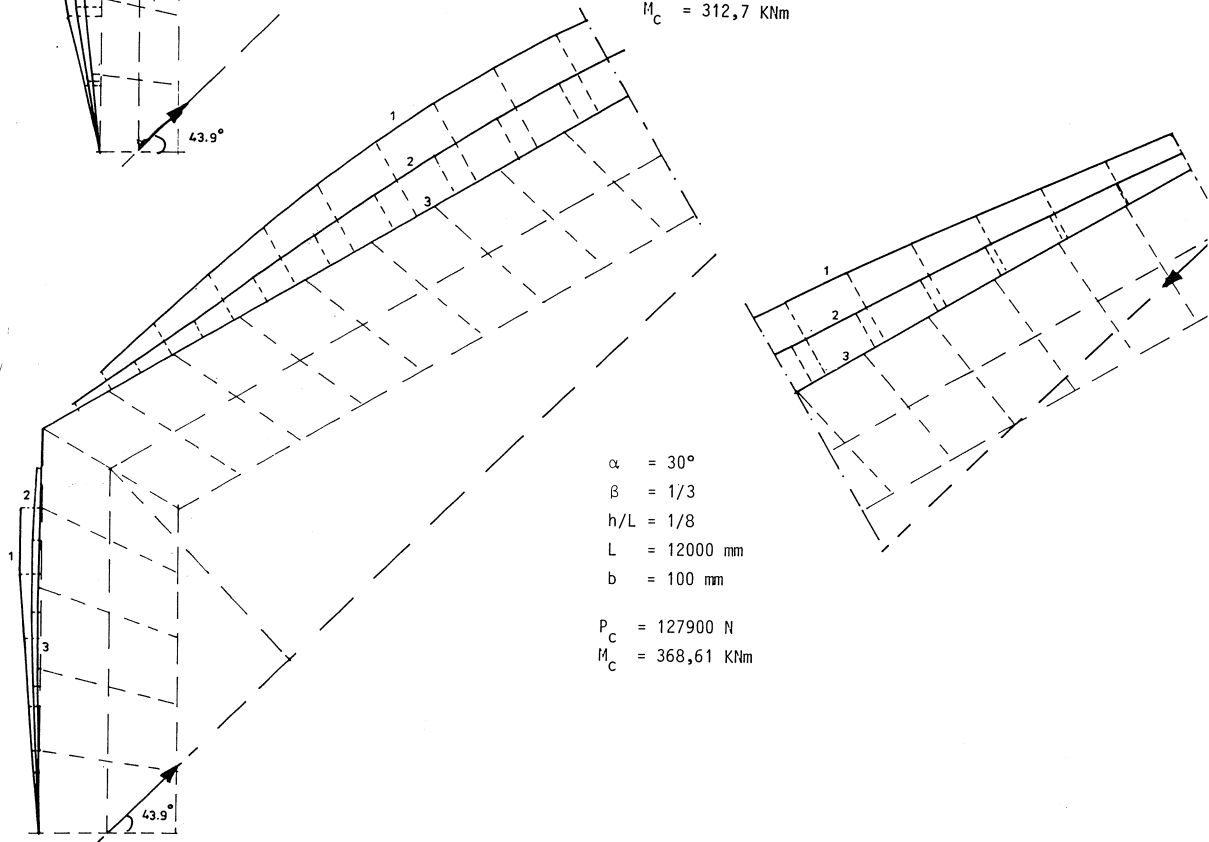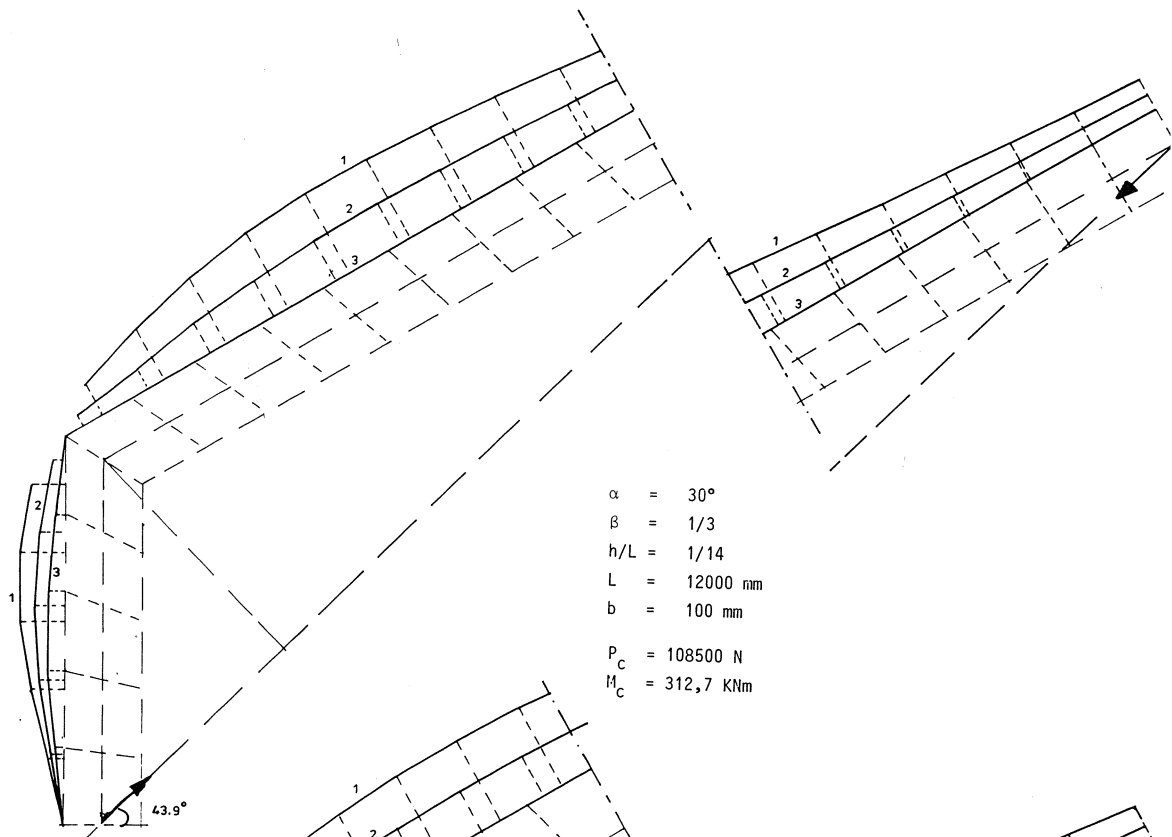
APPENDIX D

Derivation of differential equation of the schematized roof beam
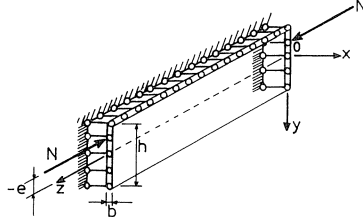

Fig. 22. Schematized roof beam.

The potential energy (equation A5) is expressed by:

$$U_t = \int_0^L \left(\tfrac{1}{2}EI_y u''^2 + \tfrac{1}{2}GI_t \varphi'^2 + \tfrac{1}{2}EC_w \varphi''^2 - \tfrac{1}{2}Nu'^2 - \tfrac{1}{2}N\frac{I_p}{A}\varphi'^2 + M \cdot u'' \cdot \varphi \right) dz \quad \text{(D1)}$$

Furthermore:

$$u = \tfrac{1}{2}h \cdot \varphi \tag{D2}$$

Equation (D1) can then be written as:

$$U_t = \int_0^L \left\{ \tfrac{1}{2}EI_y(\tfrac{1}{2}h\varphi'')^2 + \tfrac{1}{2}GI_t \varphi'^2 + \tfrac{1}{2}EC_w \varphi''^2 - \tfrac{1}{2}N(\tfrac{1}{2}h\varphi')^2 - \tfrac{1}{2}N\frac{I_p}{A}\varphi'^2 + M \cdot \tfrac{1}{2}h\varphi'' \cdot \varphi \right\} dz \tag{D3}$$

For a state of equilibrium the following condition must be satisfied:

$$\frac{\partial(U_t)}{\partial\varphi} - \frac{d}{dz}\left[\frac{\partial(U_t)}{\partial\varphi'}\right] + \frac{d}{dz^2}\left[\frac{\partial(U_t)}{\partial\varphi''}\right] = 0 \tag{D4}$$

Differentiation of (D3) enables (D4) to be written as:

$$\tfrac{1}{4}h^2 EI_y \varphi'''' + EC_w \varphi'''' - GI_t \varphi'' + N \cdot \tfrac{1}{4}h^2 \varphi'' + N \cdot \frac{I_p}{A} \cdot \varphi'' + M \cdot \tfrac{1}{2}h \cdot \varphi'' + M \cdot \tfrac{1}{2}h \cdot \varphi'' \tag{D5}$$

For narrow rectangular cross-sections I_p is approximately $bh^3/12$ so that equation (D5) can be written as:

$$\left(EI_y \cdot \tfrac{1}{4}h^2 + EC_w\right)\varphi'''' + \left(\tfrac{1}{3}h^2 N + hM - GI_t\right)\varphi'' = 0 \tag{D6}$$

and with $M = N \cdot e$ this equation can be written as:

$$\left(EI_y \cdot \tfrac{1}{4}h^2 + EC_w\right)\varphi'''' + \left(\tfrac{1}{3}h^2 N + h \cdot e \cdot N - GI_t\right)\varphi'' = 0 \tag{D7}$$

Solution of differential equation (D7):
For narrow rectangular cross-sections:

$$EC_w \approx \tfrac{1}{144}b^3 h^3 \tag{D8}$$

41

so that (D7) can be written as:

$$(\tfrac{1}{36}b^3h^3 \cdot E)\varphi'''' + (\tfrac{1}{3}h^2N + h \cdot e \cdot N - GI_t)\varphi'' = 0 \tag{D9}$$

Put

$$\varphi = A \sin \frac{\pi}{L} z \tag{D10}$$

$$\varphi'' = \frac{\pi^2}{L^2} A \sin \frac{\pi}{L} z \quad \text{and} \quad \varphi'''' = \frac{\pi^4}{L^4} A \sin \frac{\pi}{L} z \tag{D11}$$

Equation (D9) can now be written as:

$$(\tfrac{1}{36}b^3h^3E)\frac{\pi^4}{L^4} A \sin \frac{\pi}{L} z - \frac{\pi^2}{L^2} A \sin \frac{\pi}{L} z (\tfrac{1}{3}h^2N + h \cdot e \cdot N - GI_t) = 0 \tag{D12}$$

$$N_{kr} = \frac{\tfrac{1}{3}h^2 \dfrac{\pi^2 EI_y}{L^2} + GI_t}{\tfrac{1}{3}h^2 + h \cdot e} \tag{D13}$$

With $S = h/L$ this latter equation can be written as:

$$N_{kr} = \frac{EI_y}{L^2} \frac{\left(\pi^2 + \dfrac{12G}{ES^2}\right)}{1 + \dfrac{3e}{h}} \tag{D14}$$

For the portal frame, at the section where the maximum bending moment occurs:

$$e = L \sin \nu \tag{D15}$$

Equation (D14) can now be written as:

$$N_{kr} = P \cos \nu = \frac{EI_y}{L^2} \frac{\left(\pi^2 + \dfrac{12G}{ES^2}\right)}{\left(1 + \dfrac{3 \sin \nu}{S}\right)} \tag{D16}$$

Because of the different boundary conditions and loading, the critical load of the roof beam will differ a little from the value given by the above equation, e.g., by a factor $\delta = f(\alpha, \beta, S)$.

For the critical load of the roof beam we can then write:

$$P \cos \nu = \frac{EI_y}{L^2} \frac{\left(\pi^2 + \dfrac{12G}{ES^2}\right)}{1 + \dfrac{3 \sin \nu}{S}} * \delta \tag{D17}$$

APPENDIX E

Derivation of the differential equations of circular arch frames of bisymmetric cross-section
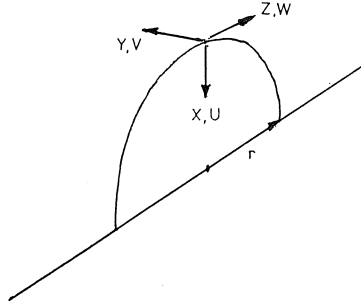

Fig. 23.   Orientation of axes.

The differential equations are derived with the aid of the principle of minimum potential energy.

Potential energy = elastic energy − work done by external load

For the circular arch in Fig. 23 the following relations can be derived:

$$\varkappa_x = \frac{\varphi_z}{r} - \frac{d^2 V_s}{ds^2}, \quad \varkappa_y = \frac{d^2 u_s}{ds^2} + \frac{d\omega_s}{ds} \cdot \frac{1}{r} + \frac{1}{r}, \quad \frac{d\Phi}{ds} = \frac{d\varphi_z}{ds} + \frac{1}{r} \cdot \frac{dV_s}{s}$$

$$\varphi_x = -\frac{dV_s}{ds}, \quad \varphi_y = \frac{du_s}{ds} + \frac{\omega_s}{r}, \quad \varepsilon_z = \frac{d\omega_s}{ds} - \frac{u_s}{r} \tag{E1}$$

If the in-plane deformations (i.e., in the plane of greatest stiffness) are neglected in relation to those perpendicular thereto, we obtain:

$$u_s = w_s = 0 \cdot \tag{E2}$$

With the aid of (E1) and (E2) the following equation can be derived for the elastic energy:

$$E_a = \frac{EI_x}{2} \int_0^1 \left(\frac{\varphi_z}{r} - \frac{d^2 V_s}{ds^2} \right)^2 ds + \frac{EC_w}{2} \int_0^1 \left(\frac{d^2 \varphi_z}{ds^2} + \frac{d^2 V_s}{ds^2} \cdot \frac{1}{r} \right)^2 ds + \frac{GI_t}{2} \int_0^1 \left(\frac{d\varphi_z}{ds} + \frac{1}{r} \frac{dV_s}{ds} \right)^2 ds \tag{E3}$$

Work done by the external load:
The work done by a fibre, of cross-sectional area dF, under the action of an external load in the plane of the arch is:

$$dA_a = dP \cdot \Delta L$$

$$dp = \sigma \cdot dF = \left(\frac{S_z}{F} - \frac{M_y}{I_y} \varkappa \right) dF \Rightarrow dA_a = \left[\left(\frac{S_z}{F} - \frac{M_y}{I_y} \varkappa \right) \Delta l \right] dF \tag{E4}$$

43

Δl is a function which depends on the displacement quantities and the co-ordinates (x, y) of the fibre in the cross-section. If the deformation in the plane of greatest stiffness is neglected in relation to the deformation at right angles thereto, the following expression can be derived for Δl:

$$\Delta l = \int_0^l \varphi_z \cdot \frac{V_s}{r}\, ds + \frac{1}{2}\int_0^l \left(\frac{dV_s}{ds}\right)^2 ds - \int_0^l \varphi_z \cdot \frac{d^2 V_s}{ds^2} \cdot \frac{x^2}{r}\, ds + \frac{1}{2}\int_0^l \left(\frac{d^2 V_s}{ds^2}\right)^2 y^2\, ds + \int_0^l \varphi_z \cdot \frac{d^2 V_s}{ds^2} \cdot \frac{y^2}{r}\, ds -$$

$$- \int_0^l \varphi_z \cdot \frac{d^2 V_s}{ds^2} x\, ds + \int_0^l \frac{x}{r}\, ds + \int_0^l \left(\frac{dV_s}{ds}\right)^2 \frac{x}{r}\, ds - \int_0^l \frac{d^2 V_s}{ds^2} y\, ds - \int_0^l \frac{\varphi_z}{r} y\, ds - \int_0^l \varphi_z \cdot \left(\frac{dV_s}{ds}\right)^2 \frac{y}{r}\, ds$$

$$- 2\int_0^l \frac{d^2 V_s}{ds^2} \frac{xy}{r}\, ds + \int_0^l \left(\frac{d^2 V_s}{ds^2}\right)^2 \frac{xy^2}{r}\, ds + \frac{1}{2}\int_0^l \left(\frac{d\Phi}{ds}\right)^2 (x^2 + y^2)\, ds - \int_0^l \frac{x}{r}\, ds - \frac{1}{2}\int_0^l \left(\frac{dV_s}{ds}\right)^2 \frac{x}{r}\, ds$$

$$- \frac{1}{2}\int_0^l \left(\frac{d^2 V_s}{ds^2}\right)^2 \frac{xy}{r}\, ds + \int_0^l \varphi_z \cdot \frac{d^2 V_s}{ds^2} \frac{x^2}{r}\, ds + \int_0^l \frac{d^2 V_s}{ds^2} \cdot \frac{xy}{r}\, ds \qquad (E5)$$

The derivations of the equations (E5) and (E8) are lengthy and have therefore been omitted here. Readers interested in them are referred to E. Katzschner's thesis [17].

$$A_a = \int_F dA = \int_F P \cdot \Delta l = \int_F \left[\left(\frac{S_z}{F} - \frac{M_y}{I_y} x\right) \Delta l\right] dF \qquad (E6)$$

If x and y are calculated with respect to the principal axes of the cross-section, then equation (E6) with

$$\int_F x^2\, dF + \int_F y^2\, dF = i_p^2 \cdot F \qquad (E7)$$

can be written as:

$$A_a = \int_0^l S_z \cdot \varphi_z \cdot \frac{V_s}{r}\, ds + \frac{1}{2}\int_0^l S_z \left(\frac{dV_s}{ds}\right)^2 ds + \frac{1}{2}i_p^2 \int_0^l S_z \left(\frac{d\varphi_z}{ds} + \frac{1}{r}\frac{dV_s}{ds}\right)^2 ds +$$

$$+ \int_0^l M_y \cdot \varphi_z \frac{d^2 V_s}{ds^2}\, ds - \frac{1}{2}\int_0^l M_y \left(\frac{dV_s}{ds}\right)^2 \cdot \frac{ds}{r} \qquad (E8)$$

The potential energy of the arch on undergoing a lateral displacement v and a rotation φ can be written as follows:

$$U_t = E_a - A_a = \frac{1}{2}\int_0^l \left[EI_x \left(-\frac{d^2 V_s}{ds^2} + \frac{\varphi_z}{r}\right)^2 + EC_w \left(\frac{d^2 \varphi_z}{ds^2} + \frac{d^2 V_s}{ds^2} \cdot \frac{1}{r}\right)^2 + GI_t \left[\left(\frac{d\varphi_z}{ds}\right)^2 + \right. \right.$$

$$+ 2\left(\frac{d\varphi_z}{ds} \cdot \frac{dV_s}{ds} \cdot \frac{1}{r}\right) + \left(\frac{dV_s}{ds} \cdot \frac{1}{r}\right)^2\right] - 2S_z \cdot \varphi_z \cdot \frac{V_s}{r} - S_z \left(\frac{dV_s}{ds}\right)^2 -$$

$$- i_p^2 S_z \left(\frac{d\varphi_z}{ds} + \frac{1}{r}\cdot\frac{dV_s}{ds}\right)^2 - 2M_y \varphi_z \frac{d^2 V_s}{ds^2} + M_y \left(\frac{dV_s}{ds}\right)^2 \cdot \frac{1}{r}\right] ds \qquad (E9)$$

44

Introducing $GI_{t\,red} = GI_t - S_z \cdot i_p^2$, the term under the integral sign in equation (E9) can be written as:

$$\left[EI_x \left(-\frac{d^2 V_s}{ds^2} + \frac{\varphi_z}{r} \right)^2 + EC_w \left(\frac{d^2 \varphi_z}{ds^2} + \frac{d^2 V_s}{ds^2} \cdot \frac{1}{r} \right)^2 + GI_{t\,red} \left(\frac{d\varphi_z}{ds} \right)^2 + 2 \frac{GI_{t\,red}}{r} \cdot \frac{d\varphi_z}{ds} \cdot \frac{dV_s}{ds} + \right.$$

$$\left. + \frac{GI_{t\,red}}{r^2} \left(\frac{dV_s}{ds} \right)^2 - 2 S_z \varphi_z \frac{V_s}{r} - S_z \left(\frac{dV_s}{ds} \right)^2 - 2 M_y \varphi_z \frac{d^2 V_s}{ds^2} + M_y \left(\frac{dV_s}{ds} \right)^2 \cdot \frac{1}{r} \right] \tag{E10}$$

If the displaced and rotated position of the arch represents a state of equilibrium, then:

$$\delta u_t = 0 \tag{E11}$$

With the aid of the calculus of variations it can be shown that this condition is satisfied if:

$$\int_0^1 \left[\frac{\partial D}{\partial V_s} \, \delta V_s + \frac{\partial D}{\partial V_s'} \, \delta V_s' + \frac{\partial D}{\partial V_s''} \, \delta V_s'' \right] ds = 0 \tag{E12}$$

and

$$\int_0^1 \left[\frac{\partial D}{\partial \varphi_z} \, \delta \varphi_z + \frac{\partial D}{\partial \varphi_z'} \, \delta \varphi_z' + \frac{\partial D}{\partial \varphi_z''} \, \delta \varphi_z'' \right] ds = 0 \tag{E13}$$

$D = U_t$ see equation E9

Applying partial integration, the following differential equations and boundary conditions can be derived from (E12) and (E13):

1. $EI_x \left(\dfrac{d^4 V_s}{ds^4} - \dfrac{d^2 \varphi_z}{ds^2} \cdot \dfrac{1}{r} \right) + EC_w \left(\dfrac{d^4 \varphi_z}{ds^4} \cdot \dfrac{1}{r} + \dfrac{d^4 V_s}{ds^4} \cdot \dfrac{1}{r^2} \right) - \dfrac{GI_{t\,red}}{r} \left(\dfrac{d^2 \varphi_z}{ds^2} + \dfrac{d^2 V_s}{ds^2} \cdot \dfrac{1}{r} \right) -$

$$- \frac{d^2 V_s}{ds^2} \left(\frac{M_y}{r} - S_z \right) - \frac{d^2}{ds^2} (M_y \cdot \varphi_z) + 2 S_x \frac{d^2 V_s}{ds} \cdot \frac{1}{r} - S_z \varphi_z \cdot \frac{1}{r} = 0 \tag{E14}$$

2. $EC_w \left(\dfrac{d^4 \varphi_z}{ds^4} + \dfrac{d^4 V_s}{ds^4} \cdot \dfrac{1}{r} \right) - GI_{t\,red} \left(\dfrac{d^2 \varphi_z}{ds^2} + \dfrac{d^2 V_s}{ds^2} \cdot \dfrac{1}{r} \right) - EI_x \left(\dfrac{d^2 V_s}{ds^2} \cdot \dfrac{1}{r} - \dfrac{\varphi_z}{r^2} \right) -$

$$- \frac{d^2 V_s}{ds^2} M_y + \frac{M_y}{r} \cdot \varphi_z \tag{E15}$$

The following relationships are incorporated in these equations:

$$\frac{dM_y}{ds} = -S_x, \quad \frac{dS_z}{ds} = S_x \cdot \frac{1}{r} \quad \text{and} \quad M_y = -S_z \cdot r \tag{E16}$$

Boundary conditions:

$$\left[EI_x\left(\frac{d^2V_s}{ds^2}-\frac{\varphi_z}{r}\right)+EC_w\left(\frac{d^2\varphi_z}{ds^2}\cdot\frac{1}{r}+\frac{d^2V_s}{ds^2}\cdot\frac{1}{r^2}\right)-(M_y\varphi_z)\right]\delta V_s'\Big|_{s=0}^{s=1}-\left[EI_x\left(\frac{d^3V_s}{ds^3}-\frac{d\varphi_z}{ds}\cdot\frac{1}{r}\right)\right.$$

$$+EC_w\left(\frac{d^3\varphi_z}{ds^3}\cdot\frac{1}{r}+\frac{d^3V_s}{ds^3}\cdot\frac{1}{r^2}\right)-M_y\frac{d\varphi_z}{ds}-\frac{GI_{t\,red}}{r}\left(\frac{d\varphi_z}{ds}+\frac{1}{r}\cdot\frac{dV_s}{ds}\right)+$$

$$+S_z\frac{dV_s}{ds}-M_y\frac{dV_s}{ds}\cdot\frac{1}{r}\left.\right]\delta V_s\Big|_{s=0}^{s=1} \tag{E17}$$

$$\left[EC_w\left(\frac{d^2\varphi_z}{ds^2}+\frac{d^2V_s}{ds^2}\cdot\frac{1}{r}\right)\right]\delta\varphi_z'\Big|_{s=0}^{s=1}-\left[EC_w\left(\frac{d^3\varphi_z}{ds^3}+\frac{d^3V_s}{ds^3}\cdot\frac{1}{r}\right)-\right.$$

$$-GI_{t\,red}\left(\frac{d\varphi_z}{ds}+\frac{dV_s}{ds}\cdot\frac{1}{r}\right)\left.\right]\delta\varphi_z\Big|_{s=0}^{s=1} \tag{E18}$$

With the aid of the transformations given below, the differential equations and boundary conditions obtained can be transformed to polar co-ordinates:

$$\frac{d^nv}{ds^n}=\frac{d^nv}{d\alpha^n}\cdot\frac{1}{r^n};\quad \frac{d^n\varphi_z}{ds^n}=\frac{d^n\varphi_z}{d\alpha^n}\cdot\frac{1}{r^n};\quad \frac{d^nM}{ds^n}=\frac{d^nM}{d\alpha^n}\cdot\frac{1}{r^n} \tag{E19}$$

The new variable is $\alpha = s/r$. The derivatives with respect to α are represented by dot superscripts:

1. $EI_x\left(\dfrac{V_s^{\cdots}}{r}-\ddot{\varphi}_z\right)-GI_{t\,red}\left(\dfrac{\ddot{V}_s}{r}+\ddot{\varphi}_z\right)+EC_w\left(\dfrac{V_s^{\cdots}}{r^3}+\dfrac{\varphi_z^{\cdots}}{r^2}\right)-\dot{V}_s(M_y-S_z\cdot r)$

$$-(M_y\cdot\varphi_z)^{\cdots}r+2S_x\dot{V}_s r-S_z\varphi_z r^2=0 \tag{E20}$$

2. $EC_w\left(\dfrac{V_s^{\cdots}}{r^3}+\dfrac{\varphi_z^{\cdots}}{r^2}\right)-GI_{t\,red}\left(\dfrac{\ddot{V}_s}{r}+\ddot{\varphi}_z\right)-EI_x\left(\dfrac{\ddot{V}_s}{r}-\varphi_z\right)-\ddot{V}_s M_y+\varphi_z M_y\cdot r=0 \tag{E21}$

Boundary conditions:

$$EI_x\left(\frac{V_s^{\cdots},R}{r^2}-\frac{\dot{\varphi}_z,R}{r}\right)+EC_w\left(\frac{\varphi_z^{\cdots},R}{r^2}+\frac{V_s^{\cdots},R}{r^3}\right)-GI_{t\,red}\left(\frac{\dot{V}_s,R}{r}+\dot{\varphi}_z,R\right)-M_y\dot{\varphi}_z,R+$$

$$+S_z\dot{V}_s,Rr-M_y\dot{V}_s,R=0 \tag{E22}$$

$$EI_x\left(\frac{\ddot{V}_s,R}{r}-\varphi_z,R\right)+EC_w\left(\frac{\ddot{\varphi}_z,R}{r}+\frac{\ddot{V}_s,R}{r^2}\right)-M_y\varphi_z,r=0 \tag{E23}$$

$$EC_w\left(\frac{\varphi_z^{\cdots},R}{r^2}+\frac{V_s^{\cdots},R}{r^3}\right)-GI_{t\,red}\left(\dot{\varphi}_z,R+\frac{\dot{V}_s,R}{r}\right)=0 \tag{E24}$$

$$EC_w\left(\frac{\ddot{\varphi}_z,R}{r^2}+\frac{\ddot{V}_s,R}{r^3}\right)=0 \tag{E25}$$

46

APPENDIX F

Circular arch frames with a restrained axis of rotation

If a circular arch is rigidly supported at a distance f from the centroid of its cross-section so as to prevent lateral displacement and if $f \ll r$, then:

$$V_s = \Phi f = \left(\varphi_z + \frac{V_s}{r}\right) \cdot f \Rightarrow V_s = \varphi_z \frac{rf}{r-f} \cong \varphi_z \cdot f \tag{F1}$$

With the aid of this relation the equations (E20) and (E21) can be written as:

1. $EI_x \left(\varphi_z^{::} \frac{f}{r} - \varphi_z^{\cdot\cdot}\right) - GI_{t\,red} \varphi_z^{\cdot\cdot} \left(1 + \frac{f}{r}\right) + \frac{EC_w}{r^2} \cdot \varphi_z^{::} \left(1 + \frac{f}{r}\right) - \varphi_z^{\cdot\cdot} f \left(M_y - S_z \cdot r\right) -$

$$- (M_y \varphi_z)^{\cdot\cdot} r + 2S_x f \varphi_z^{\cdot} r - S_z \cdot \varphi_z \cdot r^2 = 0 \tag{F2}$$

2. $EC_w \cdot \frac{1}{r^2} \cdot \varphi_z^{::} \left(1 + \frac{f}{r}\right) - GI_{t\,red} \varphi_z^{\cdot\cdot} \left(1 + \frac{f}{r}\right) - EI_x \left(\varphi_z^{\cdot\cdot} \frac{f}{r} - \varphi_z\right) -$

$$- M_y \cdot f \cdot \varphi_z^{\cdot\cdot} + M_y \cdot r \cdot \varphi_z = 0 \tag{F3}$$

By multiplying (F3) by f/r it becomes possible to combine (F2) and (F3) into the following differential equation:

$$\frac{EC_w}{r^2} \varphi_z^{::} \left(1 + \frac{f}{r}\right)^2 - GI_{t\,red} \cdot \varphi_z^{\cdot\cdot} \left(1 + \frac{f}{r}\right)^2 + EI_x \left(\varphi_z^{::} \frac{f^2}{r^2} - 2\frac{f}{r} \varphi_z^{\cdot\cdot} + \varphi_z\right) - (M_y \varphi_z)^{\cdot\cdot} f +$$

$$+ S_z f^2 \varphi_z^{\cdot\cdot} + 2S_x f^2 \varphi_z^{\cdot} - S_z \cdot f \cdot r \cdot \varphi_z - M_y \varphi_z^{\cdot\cdot} f \left(1 + \frac{f}{r}\right) + M_y \cdot r \cdot \varphi_z = 0 \tag{F4}$$

For the structure shown in Fig. 24 equation (F4) can, by making use of symmetry considerations, be written as:

$$\frac{EC_w}{r^2} \varphi_z^{::} \left(1 + \frac{f}{r}\right)^2 - GI_{t\,red} \cdot \varphi_z^{\cdot\cdot} \left(1 + \frac{f}{r}\right)^2 + EI_x \left(\varphi_z^{::} \frac{f^2}{r^2} - 2\frac{f}{r} \varphi_z^{\cdot\cdot} + \varphi_z\right) +$$

$$+ P \cdot r \cdot f \cdot \left(2 + \frac{f}{r}\right) \left(\cos \alpha - \cos \frac{\alpha_0}{2}\right) \varphi_z^{\cdot\cdot} - Pf^2 \cos \alpha \varphi_z^{\cdot\cdot} - 2Prf \left(1 + \frac{f}{r}\right) \sin \alpha \varphi_z^{\cdot} -$$

$$- P \cdot r^2 \left(\cos \alpha - \cos \frac{\alpha_0}{2}\right) \varphi_z = 0 \tag{F5}$$

$$S_z = - P \cos \alpha \tag{F6}$$

$$S_x = - P \sin \alpha \tag{F7}$$

$$M_y = - P \cdot r \cdot \left(\cos \alpha - \cos \frac{\alpha_0}{2}\right) \tag{F8}$$

$$M_y^{\cdot} = P \cdot r \cdot \sin \alpha \tag{F9}$$

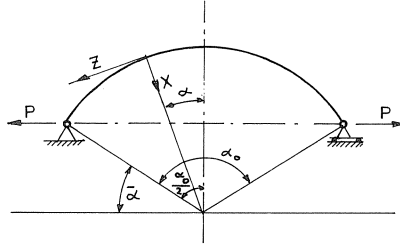$$M_y^{\cdot\cdot} = P \cdot r \cdot \cos \alpha \tag{F10}$$

Fig. 24. Schematic of arch frame.

Katzschner obtains an approximate solution to this differential equation with the aid of Galerkin's method. For this purpose an approximation for φ is provided by the following series:

$$\bar{\varphi}_z = \sum_{i=1}^{n} b_i z(\alpha) \tag{F11}$$

In this formula b_i is a constant and $z(\alpha)$ a function which satisfies the boundary conditions applicable to the case.

These boundary conditions are:

$$\varphi_z \left(\frac{\alpha_0}{2} \right) = 0; \quad \varphi_{\ddot{z}} \left(\frac{\alpha_0}{2} \right) = 0; \quad \varphi_z \left(-\frac{\alpha_0}{2} \right) = 0 \quad \text{and} \quad \varphi_{\ddot{z}} \left(-\frac{\alpha_0}{2} \right) = 0 \tag{F12}$$

For an arch loaded in tension Katzschner chooses the following expression for φ:

$$\bar{\varphi}_z = b_1 \sin 2k\pi \frac{\alpha}{\alpha_0}; \qquad k = 1, 2, \dots \tag{F13}$$

whence follows:

$$\bar{\varphi}_{\dot{z}} = b_1 \, 2k \, \frac{\pi}{\alpha_0} \cos 2k\pi \frac{\alpha}{\alpha_0} \tag{F14}$$

$$\bar{\varphi}_{\ddot{z}} = -b_1 \, 4k^2 \frac{\pi^2}{\alpha_0^2} \sin 2k\pi \frac{\alpha}{\alpha_0} \tag{F15}$$

$$\bar{\varphi}_{\dddot{z}} = -b_1 \, 8k^3 \frac{\pi^3}{\alpha_0^3} \cos 2k\pi \frac{\alpha}{\alpha_0} \tag{F16}$$

$$\varphi_{\ddddot{z}} = b_1 16k^4 \frac{\pi^4}{\alpha_0^4} \sin 2k\pi \frac{\alpha}{\alpha_0} \tag{F17}$$

The following expressions will now be introduced:

$$a_1 = \frac{EC_w}{r^2} \left(1 + \frac{f}{r} \right)^2 + EI_x \frac{f^2}{r^2} \tag{F18}$$

$$a_2 = GI_{t\,red} \left(1 + \frac{f}{r} \right)^2 + 2 \frac{f}{r} EI_x \tag{F19}$$

48

$$a_3 = f\left(2 + \frac{f}{r}\right) \tag{F20}$$

$$a_4 = EI_x \tag{F21}$$

With the aid of these expressions the equation (F5) can be written as:

$$a_1\varphi_{\ddot{z}} - a_2\varphi_{\ddot{z}} + a_4\varphi_z + P\cdot r\left\{\left[a_3\left(\cos\alpha - \cos\frac{\alpha_0}{2}\right) - \frac{f^2}{r}\cos\alpha\right]\varphi_{\ddot{z}} - \right.$$

$$\left. - 2f\left(1 + \frac{f}{r}\right)\sin\alpha\cdot\varphi_{\dot{z}} - r\left(\cos\alpha - \cos\frac{\alpha_0}{2}\right)\varphi_z\right\} = 0 \tag{F22}$$

Basing ourselves on the limits of integration $\alpha = 0$ and $\alpha = \alpha_0/2$, we obtain for the "Galerkin" equation:

$$b_1\int\limits_{\alpha=0}^{\alpha=\frac{\alpha_0}{2}}\left\{a_1 16k^4\frac{\pi^4}{\alpha_0^4}\sin^2 2k\pi\frac{\alpha}{\alpha_0} + a_2 4k^2\frac{\pi^2}{\alpha_0^2}\sin^2 2k\pi\frac{\alpha}{\alpha_0} + a_4\sin^2 2k\pi\frac{\alpha}{\alpha_0} + \right.$$

$$+ P\cdot r\left[4a_3 k^2\frac{\pi^2}{\alpha_0^2}\left(-\cos\alpha\sin^2 2k\pi\frac{\alpha}{\alpha_0} + \cos\frac{\alpha_0}{2}\cdot\sin^2 2k\pi\frac{\alpha}{\alpha_0} + \right.\right.$$

$$+ 4\frac{f^2}{r}k^2\frac{\pi^2}{\alpha_0^2}\cos\alpha\sin^2 2k\pi\frac{\alpha}{\alpha_0} - 4f\left(1 + \frac{f}{r}\right)k\frac{\pi}{\alpha_0}\sin\alpha\cos 2k\pi\frac{\alpha}{\alpha_0}\sin 2k\pi\frac{\alpha}{\alpha_0} - $$

$$\left.\left.\left. - r\cos\alpha\sin^2 2k\pi\frac{\alpha}{\alpha_0} + r\cos\frac{\alpha_0}{2}\sin^2 2k\pi\frac{\alpha}{\alpha_0}\right]\right\}\,d\alpha = 0 \tag{F23}$$

Besides the trivial solution $b_1 = 0$ there is an eigenvalue if the integral is equal to zero.

With the aid of the following definite integrals the expression for the critical load can be written as equation (F27):

$$\int\limits_{\alpha=0}^{\alpha=\frac{\alpha_0}{2}}\sin^2 k\pi\frac{\alpha}{\alpha_0}\,d\alpha = \frac{\alpha_0}{4} \qquad (k = 1, 2, 3, ...) \tag{F24}$$

$$\int\limits_{\alpha=0}^{\alpha=\frac{\alpha_0}{2}}\cos\alpha\sin^2 2k\pi\frac{\alpha}{\alpha_0}\,d\alpha = \frac{1}{2}\sin\frac{\alpha_0}{2} - \frac{1}{4}\left[\frac{\sin\left(\frac{\alpha_0}{2} - 2k\pi\right)}{1 - 4k\frac{\pi}{\alpha_0}} + \frac{\sin\left(\frac{\alpha_0}{2} + 2k\pi\right)}{1 + 4k\frac{\pi}{\alpha_0}}\right] \tag{F25}$$

$$\int\limits_{\alpha=0}^{\alpha=\frac{\alpha_0}{2}}\sin\alpha\sin 2k\pi\frac{\alpha}{\alpha_0}\cos 2k\pi\frac{\alpha}{\alpha_0}\,d\alpha = \frac{1}{4}\left[\frac{\sin\left(\frac{\alpha_0}{2} - 2k\pi\right)}{1 - 4k\frac{\pi}{\alpha_0}} - \frac{\sin\left(\frac{\alpha_0}{2} + 2k\pi\right)}{1 + 4k\frac{\pi}{\alpha_0}}\right] \tag{F26}$$

49

$$a_1 4k^4 \frac{\pi^4}{\alpha_0^3} + a_2 k^2 \frac{\pi^2}{\alpha_0} + a_4 \frac{\alpha_0}{4} + P \cdot r \left[2a_3 k^2 \frac{\pi^2}{\alpha_0^2} \left(-\sin\frac{\alpha_0}{2} + \frac{1}{2}\frac{\sin\left(\frac{\alpha_0}{2} - 2k\pi\right)}{1 - 4k\frac{\pi}{\alpha_0}} + \right. \right.$$

$$\left. + \frac{1}{2}\frac{\sin\left(\frac{\alpha_0}{2} + 2k\pi\right)}{1 + 4k\frac{\pi}{\alpha_0}} + \frac{\alpha_0}{2}\cos\frac{\alpha_0}{2}\right) + 2\frac{f^2}{r}k^2\frac{\pi^2}{\alpha_0^2}\left(\sin\frac{\alpha_0}{2} - \frac{1}{2}\frac{\sin\left(\frac{\alpha_0}{2} - 2k\pi\right)}{1 - 4k\frac{\pi}{\alpha_0}} - \right.$$

$$\left. - \frac{1}{2}\frac{\sin\left(\frac{\alpha_0}{2} + 2k\pi\right)}{1 + 4k\frac{\pi}{\alpha_0}}\right) - f\left(1 + \frac{f}{r}\right)k\frac{\pi}{\alpha_0}\left(\frac{\sin\left(\frac{\alpha_0}{2} - 2k\pi\right)}{1 - 4k\frac{\pi}{\alpha_0}} - \frac{\sin\left(\frac{\alpha_0}{2} + 2k\pi\right)}{1 + 4k\frac{\pi}{\alpha_0}}\right) -$$

$$- \frac{r}{2}\left(\sin\frac{\alpha_0}{2} - \frac{1}{2}\frac{\sin\left(\frac{\alpha_0}{2} - 2k\pi\right)}{1 - 4k\frac{\pi}{\alpha_0}} - \frac{1}{2}\frac{\sin\left(\frac{\alpha_0}{2} + 2k\pi\right)}{1 + 4k\frac{\pi}{\alpha_0}}\right) + \frac{r}{4}\alpha_0\cos\frac{\alpha_0}{2}\right] = 0 \tag{F27}$$

Since $f \ll r$, the quotients of f and r (f/r) can be neglected, so that (F18), (F19) and (F20) are then changed as follows:

$$a_1 \Rightarrow \bar{a}_1 = \frac{EC_w}{r^2}; \quad a_2 \Rightarrow \bar{a}_2 = GI_{t\,red}; \quad a_3 \Rightarrow 2f \tag{F28}$$

The least eigenvalue (P_k) is obtained for $k = 1$.

With the aid of the above derivations for following expression is obtained from P_k:

$$P_k = \frac{\bar{a}_1 \cdot 4 \cdot \dfrac{\pi^4}{\alpha_0^3} + \bar{a}_2 \cdot \dfrac{\pi^2}{\alpha_0} + a_4 \cdot \dfrac{\alpha_0}{4}}{r\left[4f\dfrac{\pi^2}{\alpha_0^2}\left(\sin\dfrac{\alpha_0}{2} - \dfrac{1}{2}\dfrac{\sin\left(2\pi - \dfrac{\alpha_0}{2}\right)}{4\dfrac{\pi}{\alpha_0} - 1} - \dfrac{1}{2}\dfrac{\sin\left(2\pi + \dfrac{\alpha_0}{2}\right)}{4\dfrac{\pi}{\alpha_0} + 1} - \dfrac{\alpha_0}{2}\cos\dfrac{\alpha_0}{2}\right) + \cdots \right]}$$

$$+ f\frac{\pi}{\alpha_0}\left[\frac{\sin\left(2\pi - \frac{\alpha_0}{2}\right)}{4\frac{\pi}{\alpha_0} - 1} - \frac{\sin\left(2\pi + \frac{\alpha_0}{2}\right)}{4\frac{\pi}{\alpha_0} + 1}\right] + \frac{r}{2}\left(\sin\frac{\alpha_0}{2} - \frac{1}{2}\frac{\sin\left(2\pi - \frac{\alpha_0}{2}\right)}{4\frac{\pi}{\alpha_0} - 1} - \right.$$

$$\left. - \frac{1}{2}\frac{\sin\left(2\pi + \frac{\alpha_0}{2}\right)}{4\frac{\pi}{\alpha_0} + 1}\right) - \frac{r}{4}\alpha_0\cos\frac{\alpha_0}{2} \right] \tag{F29}$$

50

For $\alpha_0 = \pi$ this equation can be written as:

$$P_k = \frac{15\pi \left(4\bar{a}_1 + \bar{a}_2 + \dfrac{a_4}{4} \right)}{r(56f + 8r)} \tag{F30}$$

For an arch loaded in compression Katzschner chooses the following expression for φ:

$$\bar{\varphi}_z = b_1 \cos k\pi \frac{\alpha}{\alpha_0}; \quad k = 1, 3, 5, \dots \tag{F31}$$

whence follows:

$$\bar{\varphi}_z^{\cdot} = -b_1 k \frac{\pi}{\alpha_0} \sin k\pi \frac{\alpha}{\alpha_0} \tag{F32}$$

$$\bar{\varphi}_z^{\cdot\cdot} = -b_1 k^2 \frac{\pi^2}{\alpha_0^2} \cos k\pi \frac{\alpha}{\alpha_0} \tag{F33}$$

$$\bar{\varphi}_z^{\cdot\cdot\cdot} = b_1 k^3 \frac{\pi^3}{\alpha_0^3} \sin k\pi \frac{\alpha}{\alpha_0} \tag{F34}$$

$$\bar{\varphi}_z^{\cdot\cdot\cdot\cdot} = b_1 k^4 \frac{\pi^4}{\alpha_0^4} \cos k\pi \frac{\alpha}{\alpha_0} \tag{F35}$$

Basing ourselves on the limits of integration $\alpha = 0$ and $\alpha = \alpha_0/2$, we obtain for the "Galerkin" equation:

$$b_1 \int_{\alpha=0}^{\alpha=\frac{\alpha_0}{0}} \left\{ a_1 k^4 \frac{\pi^4}{\alpha_0^4} \cos^2 k\pi \frac{\alpha}{\alpha_0} + a_2 k^2 \frac{\pi^2}{\alpha_0^2} \cos^2 k\pi \frac{\alpha}{\alpha_0} + a_4 \cos^2 k\pi \frac{\alpha}{\alpha_0} - \right.$$
$$- P \cdot r \left[a_3 k^2 \frac{\pi^2}{\alpha_0^2} \left(-\cos \alpha \cos^2 k\pi \frac{\alpha}{\alpha_0} + \cos \frac{\alpha_0}{2} \cos^2 k\pi \frac{\alpha}{\alpha_0} \right) + \frac{f^2}{r} k^2 \frac{\pi^2}{\alpha_0^2} \cos \alpha \cos^2 k\pi \frac{\alpha}{\alpha_0} + \right.$$
$$+ 2f \left(1 + \frac{f}{r} \right) k \frac{\pi}{\alpha_0} \sin \alpha \sin k\pi \frac{\alpha}{\alpha_0} \cos k\pi \frac{\alpha}{\alpha_0} - r \cos \alpha \cos^2 k\pi \frac{\alpha}{\alpha_0} + $$
$$\left. \left. + r \cos \frac{\alpha_0}{2} \cos^2 k\pi \frac{\alpha}{\alpha_0} \right] \right\} d\alpha = 0 \tag{F36}$$

With the aid of the following definite integrals the expression for the critical load can be written as equation (F40):

$$\int_{\alpha=0}^{\alpha=\frac{\alpha_0}{2}} \cos^2 k\pi \frac{\alpha}{\alpha_0} \, d\alpha = \frac{\alpha_0}{4} \qquad (k = 1, 3, 5, \dots) \tag{F37}$$

51

$$\int_{\alpha=0}^{\alpha=\frac{\alpha_0}{2}} \cos\alpha\,\cos^2 k\pi\,\frac{\alpha}{\alpha_0}\,d\alpha = \tfrac{1}{2}\sin\frac{\alpha_0}{2} + \tfrac{1}{4}\left[\frac{\sin\left(\frac{\alpha_0}{2}-k\pi\right)}{1-2k\dfrac{\pi}{\alpha_0}} + \frac{\sin\left(\frac{\alpha_0}{2}+k\pi\right)}{1+2k\dfrac{\pi}{\alpha_0}}\right] \tag{F38}$$

$$\int_{\alpha=0}^{\alpha=\frac{\alpha_0}{2}} \sin\alpha\,\sin k\pi\,\frac{\alpha}{\alpha_0}\,\cos k\pi\,\frac{\alpha}{\alpha_0}\,d\alpha = \tfrac{1}{4}\left[\frac{\sin\left(\frac{\alpha_0}{2}-k\pi\right)}{1-2k\dfrac{\pi}{\alpha_0}} - \frac{\sin\left(\frac{\alpha_0}{2}+k\pi\right)}{1+2k\dfrac{\pi}{\alpha_0}}\right] \tag{F39}$$

$$a_1 k^4\frac{\pi^4}{\alpha_0^4}\frac{\alpha_0}{4} + a_2 k^2\frac{\pi^2}{\alpha_0^2}\frac{\alpha_0}{4} + a_4\frac{\alpha_0}{4} - P\cdot r\left[a_3 k^2\frac{\pi^2}{\alpha_0^2}\left(-\tfrac{1}{2}\sin\frac{\alpha_0}{2} - \tfrac{1}{4}\frac{\sin\left(\frac{\alpha_0}{2}-k\pi\right)}{1-2k\dfrac{\pi}{\alpha_0}} - \right.\right.$$

$$\left. - \tfrac{1}{4}\frac{\sin\left(\frac{\alpha_0}{2}+k\pi\right)}{1+2k\dfrac{\pi}{\alpha_0}} + \frac{\alpha_0}{4}\cos\frac{\alpha_0}{2}\right) + \frac{f^2}{r}k^2\frac{\pi^2}{\alpha_0^2}\left(\tfrac{1}{2}\sin\frac{\alpha_0}{2} + \tfrac{1}{4}\frac{\sin\left(\frac{\alpha_0}{2}-k\pi\right)}{1-2k\dfrac{\pi}{\alpha_0}} + \right.$$

$$\left. + \tfrac{1}{4}\frac{\sin\left(\frac{\alpha_0}{2}+k\pi\right)}{1+2k\dfrac{\pi}{\alpha_0}}\right) + \tfrac{1}{2}f\left(1+\frac{f}{r}\right)k\frac{\pi}{\alpha_0}\left(\frac{\sin\left(\frac{\alpha_0}{2}-k\pi\right)}{1-2k\dfrac{\pi}{\alpha_0}} - \frac{\sin\left(\frac{\alpha_0}{2}+k\pi\right)}{1+2k\dfrac{\pi}{\alpha_0}}\right) - $$

$$\left. -\frac{r}{2}\left(\sin\frac{\alpha_0}{2} + \tfrac{1}{2}\frac{\sin\left(\frac{\alpha_0}{2}-k\pi\right)}{1-2k\dfrac{\pi}{\alpha_0}} + \tfrac{1}{2}\frac{\sin\left(\frac{\alpha_0}{2}+k\pi\right)}{1+2k\dfrac{\pi}{\alpha_0}}\right) + r\frac{\alpha_0}{4}\cos\frac{\alpha_0}{2}\right] = 0 \tag{F40}$$

Again neglecting the quotients of f and r (f/r) and putting $k=1$, we obtain for the smallest critical load:

$$P_k = -\frac{\left(\bar{a}_1\dfrac{\pi^4}{\alpha_0^4} + \bar{a}_2\dfrac{\pi^2}{\alpha_0^2} + a_4\right)\alpha_0}{r\left[2f\dfrac{\pi^2}{\alpha_0^2}\left(2\sin\dfrac{\alpha_0}{2} + \dfrac{\sin\left(\pi-\frac{\alpha_0}{2}\right)}{2\dfrac{\pi}{\alpha_0}-1} + \dfrac{\sin\left(\pi+\frac{\alpha_0}{2}\right)}{2\dfrac{\pi}{\alpha_0}+1} - \alpha_0\cos\dfrac{\alpha_0}{2}\right) - \right.}$$

$$\left. -2f\dfrac{\pi}{\alpha_0}\left(\dfrac{\sin\left(\pi-\frac{\alpha_0}{2}\right)}{2\dfrac{\pi}{\alpha_0}-1} - \dfrac{\sin\left(\pi+\frac{\alpha_0}{2}\right)}{2\dfrac{\pi}{\alpha_0}+1}\right) + r\left(2\sin\dfrac{\alpha_0}{2} + \right.\right.$$

52

$$+ \frac{\sin\left(\pi - \dfrac{\alpha_0}{2}\right)}{2\dfrac{\pi}{\alpha_0} - 1} + \frac{\sin\left(\pi + \dfrac{\alpha_0}{2}\right)}{2\dfrac{\pi}{\alpha_0} + 1}\Bigg) - r\alpha_0 \cos\frac{\alpha_0}{2} \Bigg] \tag{F41}$$

For $\alpha_0 = \pi$ this equation can be written as:

$$P_{\mathrm{k}} = \frac{-3\pi\left(\bar{a}_1 + \bar{a}_2 + a_4\right)}{8r(f + r)} \tag{F42}$$